Surv Geophys (2008) 29:421–469
DOI 10.1007/s10712-008-9037-z

ORIGINAL PAPER

Estimating Land Surface Evaporation: A Review of Methods Using Remotely Sensed Surface Temperature Data

Jetse D. Kalma · Tim R. McVicar · Matthew F. McCabe

Received: 31 March 2008 / Accepted: 18 July 2008 / Published online: 12 August 2008

Abstract This paper reviews methods for estimating evaporation from landscapes, regions and larger geographic extents, with remotely sensed surface temperatures, and highlights uncertainties and limitations associated with those estimation methods. Particular attention is given to the validation of such approaches against ground based flux measurements. An assessment of some 30 published validations shows an average root mean squared error value of about 50 W m^{-2} and relative errors of 15–30%. The comparison also shows that more complex physical and analytical methods are not necessarily more accurate than empirical and statistical approaches. While some of the methods were developed for specific land covers (e.g. irrigation areas only) we also review methods developed for other disciplines, such as hydrology and meteorology, where continuous estimates in space and in time are needed, thereby focusing on physical and analytical methods as empirical methods are usually limited by in situ training data. This review also provides a discussion of temporal and spatial scaling issues associated with the use of thermal remote sensing for estimating evaporation. Improved temporal scaling procedures are required to extrapolate instantaneous estimates to daily and longer time periods and gap-filling procedures are needed when temporal scaling is affected by intermittent satellite coverage. It is also noted that analysis of multi-resolution data from different satellite/sensor systems (i.e. data fusion) will assist in the development of spatial scaling and aggregation approaches, and that several biological processes need to be better characterized in many current land surface models.

Keywords Evaporation · Remote sensing · Thermal imagery · Land surface temperature · Estimation methods · Uncertainty · Scaling

J. D. Kalma (✉)
School of Engineering, University of Newcastle, Callaghan, NSW 2308, Australia
e-mail: jetse.kalma@newcastle.edu.au

T. R. McVicar
CSIRO Land and Water and eWater CRC, GPO Box 1666, Canberra, ACT 2601, Australia

M. F. McCabe
School of Civil and Environmental Engineering, University of New South Wales, Sydney, NSW 2052, Australia

Nomenclature

B	Coefficient in Eq. 3 (−)
C_{BN}	Bulk turbulent transfer coefficient (−)
C_p	Specific heat of air at constant pressure (J kg^{-1} K^{-1})
D	Zero plane displacement height (m)
E, E_a	Actual evaporation rate (mm day^{-1})
E_n	Normalised actual evaporation (mm day^{-1})
E_p	Potential evaporation rate (mm day^{-1})
E_{PT}	Priestley–Taylor evaporation rate (mm day^{-1})
E_w	Equilibrium evaporation rate (mm day^{-1})
e_a	Actual vapour pressure of the air (Pa)
e_a*	Saturated vapour pressure of the air (Pa)
e_s*	Saturated vapour pressure at T_s (Pa)
e_u*	Saturated vapour pressure at T_u (Pa)
f_c	Fractional vegetation cover (−)
G	Soil heat flux (W m^{-2})
G_s	Surface conductance (m s^{-1})
g_b	Bulk leaf boundary layer conductance (m s^{-1})
H	Sensible heat flux (W m^{-2})
H_c	Sensible heat flux to/from canopy (W m^{-2})
H_s	Sensible heat flux to/from soil (W m^{-2})
K↓	Downwelling shortwave radiation flux (W m^{-2})
K↑	Upwelling shortwave radiation flux (W m^{-2})
k	Von Karman's constant (0.4)
kB^{-1}	Dimensionless ratio used to calculate r_{ex}
L	Monin-Obukhov length (m)
L↓	Downwelling longwave radiation flux (W m^{-2})
L↑	Upwelling longwave radiation flux (W m^{-2})
n	Exponent in Eq. 3
r_a	Aerodynamic resistance (s m^{-1})
r_c	Canopy resistance (s m^{-1})
r_{cp}	Canopy resistance at potential transpiration (s m^{-1})
r_{ex}	Excess (supplementary, extra) resistance (s m^{-1})
R_n	Net (allwave) radiation flux (W m^{-2})
$(R_n)_d$	Daily total of net radiation (W m^{-2})
r_r	Radiometric-convective resistance (s m^{-1})
r_s	Surface (stomatal, soil) resistance (s m^{-1})
T_∞	Surface temperature of very dry pixel (K; °C)
T_a	Air temperature at screen height (K; °C)
T_{aero}	Aerodynamic surface temperature (K; °C)
T_c	Canopy temperature (K; °C)
T_d	Dew point temperature (K; °C)
T_H	Surface temperature of pixel with $\lambda E = 0$ (K; °C)
$T_{\lambda E}$	Surface temperature of pixel with $H = 0$ (K; °C)
T_k	Kinetic temperature (K; °C)
T_o	Surface temperature of very wet pixel (K; °C)
T_0	Temperature of mean air stream in canopy (K; °C)
T_{rad}	Radiative surface temperature (K; °C)
T_s	Radiative surface (soil + vegetation) temperature (K; °C)

T_{soil}	Soil surface temperature (K; °C)
T_u	Unknown surface temperature in Eqs. 25 and 26 (K; °C)
T_v	Foliage (vegetation) temperature (K; °C)
u	Wind velocity (m s^{-1})
u*	Friction velocity (m s^{-1})
z_{oh}	Roughness length for sensible heat transfer (m)
z_{om}	Roughness length for momentum transfer (m)
α	Broadband albedo; hemispherical reflectance
α_{PT}	Priestley–Taylor parameter
β	Stress factor in Jiang and Islam (2003)
γ	Psychrometric constant (Pa K^{-1})
Δ	Slope of saturated vapour pressure curve at current air temperature (Pa K^{-1})
ε	Emissivity
θ	View angle
Λ	Evaporative fraction ($\lambda E/(R_n - G)$)
Λ_r	Relative evaporation (E_a/E_p)
λ	Latent heat of vaporization (J kg^{-1})
ψ_h	Stability correction for sensible heat transfer
ψ_m	Stability correction for momentum transfer
ϕ	Parameter in Eqs. 14 and 15
ρ	Air density (kg m^{-3})
ρ	Upwelling spectral reflectance (−)
Ω	Decoupling coefficient of Jarvis and McNaughton (1986)

1 Introduction

In the 1950s and 1960s evaporation[1] from well-watered land surfaces was thought to be controlled largely by meteorological conditions. Spatial variance in vegetation and soil conditions was generally not seen as important. Kalma and Calder (1994) noted that by the 1980s a number of spatially and temporally dynamic feedback mechanisms between evaporation and the land surface (e.g. surface albedo and rooting depth) were recognized. To adequately capture these feedbacks, models were developed that account for atmospheric demands, surface radiation budget and water availability, as well as a range of biological and physical interactions. Much progress has been made in gaining insight of local-scale evaporation processes through accurate point measurements with Bowen ratio and eddy correlation equipment. However, such observations only represent local processes and even measurements with advanced eddy correlation systems on towers can rarely be extended to large areas due to land surface heterogeneity and the dynamic nature of the heat transfer processes (see French et al. 2005).

Since the 1980s the general view has evolved that significant spatial variability in evaporation may be important and that effective methods for determining landscape-scale evaporation are needed. A wide range of meteorological and climatological approaches

[1] The term evaporation as used in this paper refers to what is often referred to as evapotranspiration, which includes all processes of vaporization. It is denoted as E. The equivalent latent heat flux is denoted by λE where λ is the latent heat of vaporization (J kg^{-1}). Over land surfaces the evaporation term comprises transpiration from vegetation, evaporation of water intercepted by the canopy of plants and trees, evaporation from the soil surface and evaporation from small water surfaces.

have been used to estimate areal evaporation, but it is widely recognized that there is still a paucity of (i) simulation models capable of realistically estimating the distributed nature of land surface processes; and (ii) techniques for up-scaling estimates based on point-scale observations (see also Kalma and Calder 1994). This change in view was coincident with the use of airborne eddy correlation flux apparatus, the development of scintillometry (de Bruin et al. 1996; Green et al. 2001) and especially the use of a spatially dense measurement technology—remote sensing.

Carlson (1986) discussed a range of analytical and diagnostic approaches which combine the surface energy balance expression and land surface flux equations with remotely sensed surface temperatures. The attraction of using remote sensing to monitor the land surface temperature and reflectivity (using different spectral regions) lies in its ability to: (i) spatially integrate over heterogeneous surfaces at a range of resolutions; and (ii) underpin information systems routinely generating operational areal evaporation(E) products once long time-series data availability issues are overcome (Schmidt et al. 2006).

Despite early doubts (see e.g. Shuttleworth 1991; Hall et al. 1992) about the accuracy and usefulness of satellite based radiometric temperature measurements to estimate E, over the last 15 years a wide range of remote sensing methods have been developed and evaluated. Approaches differ in: (i) type and spatial extent of application (e.g. irrigation, dry-land agriculture, forestry, hydrology or climatology [noting that the first 3 examples usually focus on specific land covers, whereas the latter two usually cover a variety of land covers]); (ii) type of remote sensing data; and (iii) use of ancillary (micro-) meteorological and land cover data.

The large number of papers published since the 1980s on the use of remotely sensed land surface temperature data to estimate E have resulted in the publication of several major reviews which report on such estimation from different perspectives. These include major overviews focusing on the use of thermal infrared radiation (TIR) data by Moran and Jackson (1991); Kustas and Norman (1996) and Quattrochi and Luval (1999). In recent years Overgaard et al. (2006) addressed the use of remote sensing from a hydrological perspective, whereas Gowda et al. (2007) and Glenn et al. (2007) focused on estimation approaches with particular reference to plant sciences, agronomy and irrigation applications. Farahani et al. (2007) surveyed progress in the measurement and modelling of crop evaporation which also includes the use of remote sensing for mapping evaporation across large areas and to a lesser extent in irrigation areas. Verstraeten et al. (2008) recently provided a comprehensive review of ground based and remote sensing methods for assessing evaporation and soil moisture content across different scales of observation.

This paper reviews methods for estimating evaporation with remotely sensed surface temperatures at local, regional and continental scales, with particular emphasis on studies published since the early 1990s. Our aim is to highlight uncertainties and limitations associated with these physical and analytical estimation methods. Particular attention is given to the validation of remote sensing techniques and land surface models against ground based flux measurements. This review also provides a discussion of temporal and spatial scaling issues associated with the use of such methods for estimating evaporation. The layout of the paper is provided in Table 1.

2 Energy Balance and Radiation Balance; Surface Temperature Measurement

Evaporation is the process whereby water is transferred from the soil and/or the vegetation layer to the atmosphere. The physical processes of evaporation and transpiration require:

Table 1 Layout of the paper, with numbers of sections and sub-sections

Section number	Topic
1	Introduction
2	Energy Balance and Radiation Balance; Surface Temperature Measurement
3	Statistical Methods using Difference Between Surface and Air Temperature
4	Surface Energy Balance Models
4.1	One-Source Surface Energy Balance Models
4.2	Two-Source Surface Energy Balance Models
5	Methods Using Time Rate of Change in Surface Temperature with Atmospheric Boundary Layer Models
6	Spatial Variability Methods
6.1	Surface Temperature, Reflectivity and Vegetation Indices
6.2	Surface Temperature and Reflectivity
6.3	Surface Temperature and Vegetation Indices
6.4	Empirical Vegetation Index Methods
7	Estimating Evaporation with Surface Temperature and Meteorological Data
7.1	Crop Water Stress and water deficit Indices
7.2	Normalised Difference Temperature Index
7.3	Methods Based on the Complementary Approach
8	Use of Remotely Sensed Surface Temperature Data with Land Surface Models
8.1	Calibration of Land Surface Models; Parameter Optimization
8.2	Data Assimilation in Land Surface Models
9	Discussion
9.1	Limitations of Estimates derived from Thermal Imagery
9.2	Evaluation of Remote Sensing Based Approaches
9.3	Temporal and Spatial Scaling Issues
10	Concluding Remarks

(i) a source of water; (ii) a source of energy; and (iii) a sink for vapour. These three requirements have led to a broad classification of methods for estimating evaporation into: (i) mass budget methods; (ii) energy budget methods; and (iii) methods based on measurements of mean profiles and atmospheric turbulence.

Surface energy balance (SEB) models are based on a solution of the surface energy budget. According to Su (2002) there are three broad SEB approaches for estimating areal evaporation. The first approach calculates the sensible heat flux (H) and then obtains the latent heat flux (λE) as the residual of the energy balance equation. This so-called residual approach is expressed by

$$\lambda E = R_n - G - H \tag{1}$$

where λE = latent heat flux, R_n = net (all-wave) radiant energy; G = soil heat flux; and H = sensible heat flux, all usually expressed in W m^{-2}. E is the rate of evaporation of water (e.g. expressed in kg m^{-2} s^{-1}) and λ = the latent heat of vaporization of water (J kg^{-1}). All terms of Eq. 1 depend on the land surface temperature. The R_n term is taken as positive if it is a gain to the surface, whereas the other fluxes are taken as positive if they are away from the surface. The second approach uses a water stress index to estimate the

relative evaporation (Λ_r), i.e. the ratio of actual to potential evaporation (E_a/E_p). E_a may then be obtained if E_p is determined from meteorological data with some type of combination equation. The third approach is to compute all components of the energy budget at the land surface with continuous Land Surface Models (LSMs) which include soil–vegetation–atmosphere transfer (SVAT) models. The ($R_n - G$) term is called the available energy. It is needed for each SEB method.

The radiation budget expressed by R_n is given by

$$R_n = K\downarrow - K\uparrow + L\downarrow - L\uparrow \quad (2)$$

where $K\downarrow$ = down-welling shortwave radiation (which depends on atmospheric transmissivity, time-of-day, day-of-year and geographic position, $K\uparrow$ = reflected shortwave radiation which depends on surface albedo (α) and $K\downarrow$, $L\downarrow$ = down-welling longwave radiation (which depends on the atmospheric emissivity which in turn is influenced by amounts of atmospheric water vapor, carbon dioxide and oxygen and by air temperature and $L\uparrow$ = up-welling longwave radiation (which depends on land surface temperature and emissivity). Readers are referred to Sellers et al. (1990); Schmugge and Becker (1991); Zhang et al. (1995); Nunez and Kalma (1995); Boegh et al. (1999) and Bisht et al. (2005) for reviews of the use of remotely sensing data for estimating components of the radiation budget and hence R_n. Bisht et al. (2005) expressed concern about the risk of error accumulation; for example, when estimating net long wave radiation the upward and downward longwave radiation fluxes are both large components, so differences between these components may be prone to significant uncertainty.

G, which is normally 5–20% of R_n during daylight hours, depends on the soil's thermal conductivity and the vertical temperature gradient, and cannot be measured remotely. Hence the ratio G/R_n is taken as constant or it is estimated as a function of several parameters, including solar zenith angle, vegetation cover, leaf area index and soil moisture status. Moran et al. (1989) and Zhang et al. (1995) used Normalised Difference Vegetation Index (NDVI)[2] data to estimate G, whereas Bastiaanssen et al. (1994, 1998a) used NDVI, surface reflectance and surface temperature as estimators and Su (2002) used fractional canopy coverage (f_c). A large numbers of studies considered the combined effect of errors in R_n and G, implying that the available energy ($R_n - G$) may be estimated with remote sensing methods to within ±10–20% (see for example Kustas and Norman 1996; Jiang et al. 2004; Bisht et al. 2005).

Land surface temperature impacts on all four terms of the energy balance of Eq. 1 and in particular on $L\uparrow$ in the radiation balance of Eq. 2. Radiative surface temperatures[3] are measured by satellite sensors such as Landsat, AVHRR, MODIS and ASTER. Quattrochi and Luval (1999) provided a brief summary of TIR theory. They note that remotely sensed surface temperature is subject to atmospheric effects which are primarily associated with the absorption of infrared radiation by atmospheric water vapor. Dash et al. (2002) and Glenn et al. (2007), amongst others, noted that early satellite sensors had errors of 3–5 K due to atmospheric effects. They note that a wide range of techniques have been developed to correct for atmospheric effects, including: (i) single-channel methods; (ii) split-window techniques; (iii) multi-angle methods; and (iv) combinations of split-window and multi-

[2] The Normalised Diffference Vegetation Index (NDVI) is defined as $[\rho_{NIR} - \rho_{RED}]/[\rho_{NIR} + \rho_{RED}]$ where ρ_{NIR} and ρ_{RED} represent the spectral reflectances in the near-infrared and red parts of the spectrum.

[3] The radiative temperature (T_{rad}) measured by an infrared radiometer from a spaceborne platform is assumed to approximate the hemispherical radiometric temperature as defined by Norman and Becker (1995).

channel methods. Description of those methods falls outside the scope of the present paper. More recently, Wan et al. (2004) described a method which uses day/night pairs of measurements in multiple infrared channels to calculate land surface temperatures. They applied this method to the MODIS 5 km land surface temperature product and reported an accuracy of ±1 K. Hook and Prata (2001) reported that the ASTER satellite sensor allows surface temperature measurements which are potentially accurate to ±0.5 K whereas Jacob et al. (2004) reported land surface temperature retrieval agreement between ASTER and MODIS of ~0.9 K. Coll et al. (2005) reported that T_{rad} retrieved from MODIS with the split-window algorithm agreed well with ground measurements with differences which were comparable with, or better than, the uncertainties in the ground measurements (a bias of 0.1°C and standard deviation of 0.6°C, for cloud free cases and viewing angles less than 60° from nadir).

3 Statistical Methods Using Difference Between Surface and Air Temperature

Early methods for estimating E from radiative temperatures were statistical approaches using linear relationships between daily totals of λE and R_n and the difference between (near) mid-day observations of T_{rad} and near-surface air temperature (T_a). Seguin and Itier (1983) proposed the following expression

$$\lambda E_d = (R_n)_d - B(T_{rad} - T_a)_i^n \quad (3)$$

where the subscripts i and d refer to instantaneous (near mid-day) and daily, respectively; B is a statistical regression coefficient which depends on surface roughness; and n depends on atmospheric stability. Equation 3 was derived from Heat Capacity Mapping Mission (HCMM) observations over fairly homogeneous irrigated and non-irrigated land surfaces, with areas between 50 and 200 km^2 (see also Seguin et al. 1982a, b). Carlson et al. (1995a) proposed a simplified method based on Eq. 3 which uses the difference between radiometric surface temperature and air temperature at 50 m at the time of the satellite overpass $(T_{rad} - T_a)_i$. They showed that B and n are closely related to fractional cover f_c which can be obtained from the NDVI–T_{rad} plots. B was found to vary from 0.015 for bare soil to 0.065 for complete vegetation cover. The exponent n decreased from 1.0 for bare soil to 0.65 for full cover. On a daily basis this method has an uncertainty of 20–30% or ±1 mm/day (Kustas and Norman 1996). It is clear that such statistical approaches require local calibration.

4 Surface Energy Balance Models

Overgaard et al. (2006) recently reviewed the evolution of land surface energy balance models since the late 1940s. These models all consider the land surface as an electrical analogue which means that the rate of exchange of a quantity (heat or mass) between two points is driven by a difference in potential (temperature or concentration) and controlled by a number of resistances that depend on the local atmospheric environment and internal properties of the land surface and vegetation.

Their review describes the development of: (i) the combination approach by Penman (1948) which assumes that the only resistance working between the wet surface and the atmosphere is the atmospheric resistance; (ii) the Penman–Monteith "one-layer",

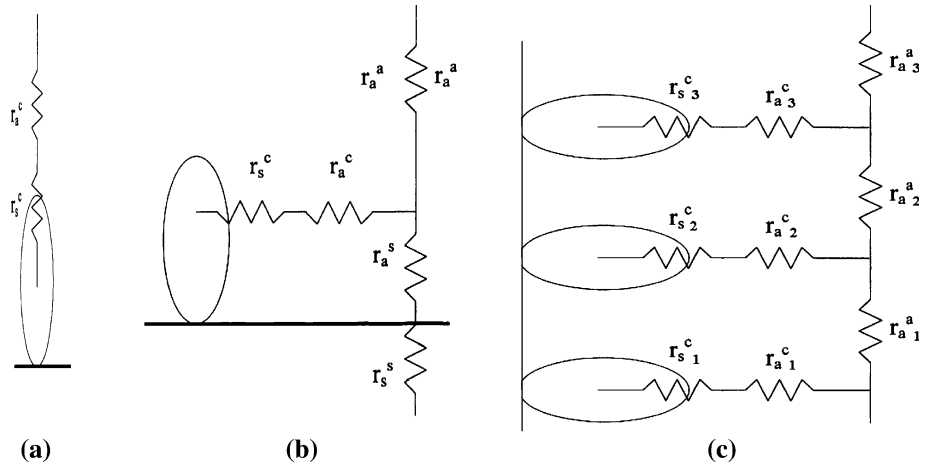

Fig. 1 Schematic diagram of the electrical resistance analogy to (**a**) one-source, (**b**) two-source and (**c**) multi-layer models, where r_a and r_s are the aerodynamic and surface resistances, and the superscripts a, c and s refer to the air, canopy and surface layers

"one-source" or "big leaf" models (Monteith 1965) which recognize the role of surface controls but do not distinguish between soil evaporation and transpiration; (iii) "two-layer" or "two-source" model such as described by Shuttleworth and Wallace (1985) which includes a canopy layer in which heat and mass fluxes from the soil and from the vegetation are allowed to interact; and (iv) multilayer models which are essentially extensions of the two-layer approach. A schematic diagram is presented in Fig. 1 which illustrates the electrical resistance analogy to: (a) one-source; (b) two-source; and (c) multi-layer models. In the following sections we discuss the use of land surface temperature observations with one-source and two-source SEB models which employ various expressions for the aerodynamic resistance to estimate the sensible heat loss from surface–air temperature differences.

4.1 One-Source Surface Energy Balance Models

A large number of one-dimensional one-source[4] SEB approaches have been reported which compute λE by evaluating R_n, G and H and solve for λE as the residual term in the energy balance equation (see Eq. 1). This involves computing the sensible heat flux H (W m^{-2}) using the electrical analogue from

$$H = \rho C_p[(T_{aero} - T_a)/r_a] \tag{4}$$

where ρ = air density (kg m^{-3}); C_p = specific heat of air at constant pressure (J kg^{-1} K^{-1}); T_{aero} = aerodynamic surface temperature[5] at canopy source/sink height (K); T_a = near-surface air temperature (K) and r_a = aerodynamic resistance to sensible heat transfer between

[4] The term one-source is used to describe models which implicitly treat the energy exchanges between soil, vegetation and the atmosphere. Such models have also been called single-layer models (see Kustas 1990).

[5] The aerodynamic surface temperature (T_{aero}) according to Norman and Becker (1995) is that temperature, which, when combined with the air temperature and a resistance calculated from the log-profile theory, provides an estimate of the sensible heat flux.

the canopy source/sink height and the bulk air at a reference height above the canopy (s m^{-1}). The r_a term is usually calculated from local data on wind speed, surface roughness length and atmospheric stability conditions.

The key issue of this approach is to estimate accurately H, as estimation (or measurement) of R_n and G is considered relatively easy (see Sect. 2). It should be noted that, although Eq. 4 is a relatively straightforward expression which makes physical sense, there are several significant difficulties in its use to estimate H (see for example Jupp and Kalma 1989; Kalma and Jupp 1990). Firstly, T_{aero} is the temperature obtained by extrapolating the logarithmic air temperature profile to the roughness length for heat transport (z_{oh}) or, more precisely, to ($d + z_{oh}$) where d = zero-plane displacement height (see Norman and Becker 1995). Because T_{aero} cannot be measured by remote sensing, it is usually replaced by T_{rad} although these two temperatures may differ by as much as 1–2 K for dense canopies and much more for sparse canopies (see Troufleau et al. 1997). Secondly, T_{rad} is related to the kinetic temperature T_k by the surface emissivity (ε) through $T_{rad} = (\varepsilon)^{1/4} T_k$. Converting radiometric temperatures to kinetic temperature requires that ε is at least considered, and preferably known. Thirdly, T_{rad} depends on view angle (θ) as discussed by Norman et al. (2000). Lastly, T_{aero} and r_a are rather difficult to obtain for non-homogeneous land surfaces and uneven terrain.

The aerodynamic resistance r_a may be calculated from

$$r_a = \left[1/k^2 u\right]\left[\ln\{(z-d)/z_{oh}\} - \Psi_h\{(z-d)/L\}\right]\left[\ln\{(z-d)/z_{om}\} - \Psi_m\{(z-d)/L\}\right] \quad (5)$$

where k = von Karman's constant (0.4); u = wind speed at reference height z (m s^{-1}); d = zero-plane displacement height (m); z_{oh} and z_{om} are the roughness lengths (m) for sensible heat and momentum flux, respectively; and Ψ_h and Ψ_m are stability correction functions for sensible heat and momentum flux, respectively, which depend on the Monin-Obukhov length L (m). These two stability functions are equal to zero if near-surface atmospheric conditions are neutrally stable. r_a is usually estimated from local data, although it must be noted that area averaging of roughness lengths is highly non-linear (see Boegh et al. 2002).

Cleugh et al. (2007) used Eqs. 1, 4 and 5 for routine monitoring of landscape-scale evaporation. Their method estimates E at 16-day intervals using 8-day composites of 1 km MODIS T_{rad} observations. The method was tested with 3 years of flux tower measurements. The 8-day composite T_{rad} values were averaged from cloud-free single-daily overpasses (acquired at about 10:30 local time) during the composite period and were aggregated from 7 × 7 pixels, yielding 49 km^2 areas centered on each flux tower. The comparisons showed significant discrepancies between observed and simulated land surface fluxes. Cleugh et al. (2007) attributed this lack of agreement to the inequality between T_{aero} and T_{rad} and to several other factors, including: (i) the estimation of H with Eqs. 4 and 5 is not constrained by the requirement for energy conservation; (ii) errors in the determination of z_{oh}; (iii) impact of errors in T_a and T_{rad}, as well as the sensitivity of H to fluctuations in r_a; (iv) use of unrepresentative emissivities; and (v) non-linearity of Eq. 4 may cause significant errors, when time-averages of instantaneous T_{rad}, T_a and R_n are used. There are two additional factors which may affect the results. Firstly, standard MODIS data processing eliminates all cloud-contaminated pixels in the composite period. T_{rad} values used in the study were therefore averages of between 0 and 8 values and were not necessarily representative of entire 8-day periods. Secondly, there is the issue of spatial representativeness of the flux tower data and the local meteorological forcing for the 49 km^2 surrounding the flux towers.

To account for the differences between T_{aero} and T_{rad}, which may be significant and amount to several degrees, especially for incomplete vegetation covers, Bastiaanssen et al. (1998a) developed an image-based calibration procedure, whereas Huang et al. (1993) developed an empirical formula to estimate T_{aero}. Others have made empirical adjustments to r_a which is related to $z_{oh.}$ For example, Stewart et al. (1994) and Kustas et al. (2003a) rewrote Eq. 4 as

$$H = \rho C_p[(T_{rad}(\theta) - T_a)/(r_a + r_{ex})] \tag{6}$$

where T_{rad} (θ) is the radiometric surface temperature (K) at view angle θ derived from the satellite brightness temperature and r_{ex} is a so-called excess resistance (s m^{-1}) which reflects differences between momentum and sensible heat transfer; all other terms are as previously defined. Stewart et al. (1994) related r_{ex} to the ratio of roughness lengths for momentum z_{om} and for sensible heat z_{oh} and the friction velocity u* (m s^{-1}) with the expression

$$r_{ex} = kB^{-1}/(ku^*) = \ln(z_{om}/z_{oh})/(ku^*) \tag{7}$$

where the kB^{-1} parameter is a dimensionless ratio determined by local calibration. Equation 7 assumes that the ratio z_{om}/z_{oh} may be treated as constant over uniform surfaces, although kB^{-1} has been found to be highly variable (see for example Brutsaert 1999).

The one-dimensional Surface Energy Balance System (SEBS) of Su (2002) estimates surface heat fluxes from satellite data and routinely available meteorological data. SEBS requires three sets of input data. The first set consists of α, ε, T_{rad}, LAI, fractional vegetation coverage and the vegetation height. When vegetation information is not explicitly available, the NDVI is used as a surrogate. The second set includes observations of T_a, u, actual vapour pressure (e_a) at a reference height as well as total air pressure. The third set of data includes measured (or estimated) K↓ and L↓. SEBS consists of several separate modules to estimate R_n, G, and the partitioning of ($R_n - G$) into H and λE. H is solved using Monin–Obukhov similarity theory. When u and vegetation parameters (height and LAI) are available, the model proposed by Massman (1997) is employed to estimate the displacement height (d) and the roughness height for momentum (z_{om}). If only the height of the vegetation is available, the relationships proposed by Brutsaert (1982, 1999) are used. SEBS has been evaluated over agricultural, grassland and forested sites and across several spatial scales. It has been used with tower based data (see Fig. 2) and with Landsat, ASTER and MODIS satellite data (McCabe and Wood 2006; Su et al. 2005, 2007) (see Fig. 6).

In Fig. 3a data from Su et al. (2005) shows good agreement between evaporation estimates over agricultural fields (corn and soy-bean) using Landsat data and in situ tower based eddy-covariance measurements.

The energy balance method used by Boegh et al. (2002) eliminated the need for an excess resistance, deriving spatial estimates of r_a, r_s and λE directly from Landsat-5 TM data. Their method uses remote sensing data with three equations to directly solve for r_a, r_s and e_a at a reference height, employing an iterative technique to estimate r_a so there is no need to estimate surface parameters, or empirically adjusted kB^{-1} values. The authors suggested that their method may be useful for larger scale applications, because it avoids the difficult task of aggregating surface parameters to a larger scale.

Estimates of λE obtained as the residual of the energy balance contain biases from both H and ($R_n - G$). Kustas (2000) identified several factors which impact on the performance of single-source approaches. Firstly, there are uncertainties about atmospheric and

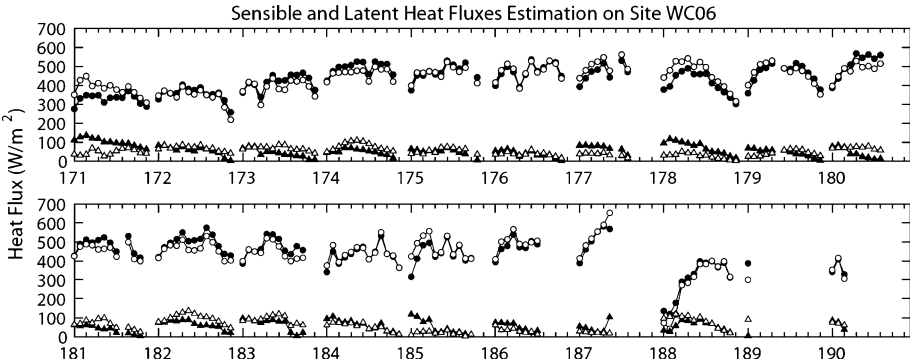

Fig. 2 Reproduction of surface flux development with a one-source model (SEBS). The time series, determined during the SMACEX-02 field experiment (Kustas et al. 2005) illustrates latent (O) and sensible (Δ) heat fluxes measured with in-situ eddy-covariance equipment (closed) together with SEBS model estimates (open) at a corn site in Iowa. Data are shown for the daytime period (1000–1600 CST), with major tick marks indicating the first morning measurement. Gaps in the time series are caused by either the absence of flux measurements or missing ancillary data (graphic derived from Su et al. 2005)

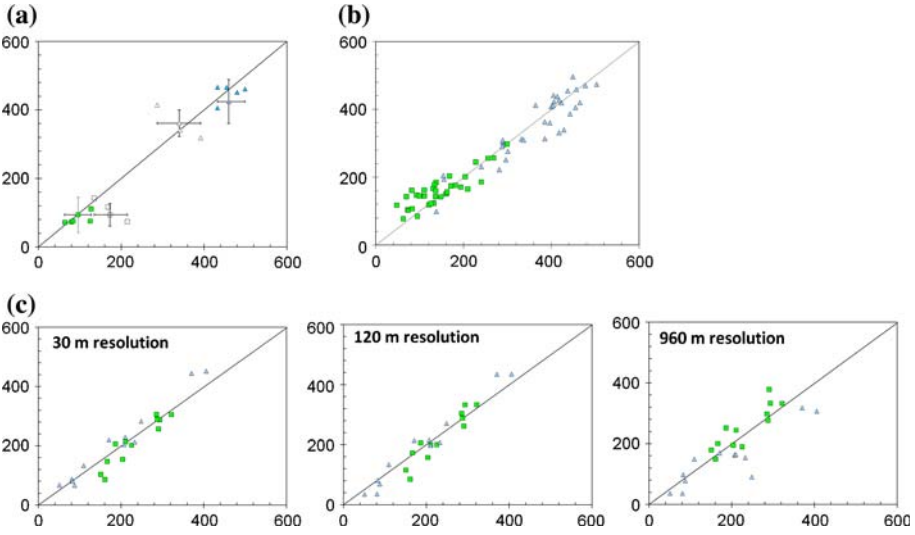

Fig. 3 Comparisons of modeled remotely sensed surface heat fluxes (vertical-axis) with in-situ eddy-covariance based tower measurements (horizontal axis). In all instances, squares represent sensible heat (H) and triangles latent heat (λE) in W m^{-2}. (**a**) is derived from Fig. 4 in Su et al. (2005) and shows Landsat based estimates from the SEBS model (Su 2002), with corn crop fluxes presented as closed symbols and soybean estimates as open symbols. The range of results present in the eddy-covariance tower observations are shown in the x-error bars and the standard deviation of satellite based estimates across the region in y-error bars. The regional average heat flux is the intersection of these lines. (**b**) is a compilation of data from Anderson et al. (2007) presenting flux results from the 1997 Southern Great Plains (SGP-97) experiment (see Jackson et al. 1999), OASIS data (see Brotzge et al. 1999) and SMACEX (see Kustas et al. 2005) using the DisALEXI approach (see Norman et al. 2003). Observations are presented across different land surface types including rangeland, pasture, corn and soybean. (**c**) is derived from Fig. 8 of Li et al. (2008), and illustrates the influences of scale on flux estimation with the TSM model (Norman et al. 1995; Kustas and Norman 1999). Here, flux estimates are calculated at three resolutions (30 m, 90 m and 960 m) using Landsat data across three different sites in southern Arizona during the SMEX-04 field campaign

emissivity effects. Secondly, as mentioned above, there is the non-uniqueness of the relationship between T_{aero} and T_{rad} due to θ and vegetation properties. Thirdly, these methods require representative near-surface T_a and other meteorological variables measured (or estimated) at the time of the satellite overpass at a location which is close to that of the T_{rad} observation. There may be significant errors involved in defining meteorological variables for each satellite pixel from a sparse network of weather stations (at the time of satellite overpass), especially in environments with high relative relief and slopes (McVicar et al. 2007a). Finally, the accuracy of any of the estimates also depends on the performance of the temperature retrieval algorithm used (e.g. Prata 1993, 1994).

4.2 Two-Source Surface Energy Balance Models

The approach represented by Eqs. 4 and 6 makes no distinction between evaporation from the soil surface and transpiration from the vegetation; therefore the resistances are not well defined (Raupach and Finnigan 1988). To address these concerns, two-source models[6] have been developed for use with incomplete canopies (e.g. Lhomme et al. 1994; Norman et al. 1995; Jupp et al. 1998; Kustas and Norman 1999). Such models treat E as the sum of evaporation from the soil surface and transpiration from vegetation. Norman et al. (1995) developed a two-source model (TSM) based on single-time observations which eliminates the need for r_{ex} as used in Eqs. 6 and 7. In its original form TSM is applicable strictly at scales of less than 10 km. Norman et al. rewrite Eq. 4 as

$$H = \rho C_p[(T_{rad}(\theta) - T_a)/(r_r)] \tag{8}$$

where $T_{rad}(\theta)$ is the directional radiometric surface temperature obtained at zenith view angle θ, and r_r is a radiometric-convective resistance (s m^{-1}) given as

$$r_r = (T_{rad}(\theta) - T_a)/[(T_c - T_a)/r_a + (T_s - T_a)/(r_a + r_s)] \tag{9}$$

In Eq. 9 T_c is the canopy temperature, T_s the soil (surface) temperature and r_s the soil resistance to heat transfer (s m^{-1}). The fractional vegetation cover (f_c) which depends on sensor view angle was used to estimate T_c and T_s from T_{rad} (θ) with

$$T_{rad}(\theta) \approx \left[f_c(\theta)T_c^4 + \{1 - f_c(\theta)\}T_s^4\right]^{1/4} \tag{10}$$

H is partitioned between the vegetated canopy (H_c) and the soil (H_s), taken in series, so that the resistance network (see Fig. 1) permits interaction between these fluxes, thus influencing the temperature in the canopy air-space.

Revisions continue to be made to TSM (see Kustas and Norman 1999; Norman et al. 2000; Kustas et al. 2003b; Li et al. 2005; Sanchez et al. 2007; 2008). Li et al. (2006) compared flux estimates from two TSM versions where: (i) thermal imagery was used to constrain T_{rad} and H; and (ii) microwave remote sensing was employed to constrain near-surface soil moisture. The estimates obtained with the two model versions were compared with flux tower observations. The results showed opposing biases for the two versions, suggesting that there may be value in combining microwave and thermal remote sensing constraints on H and λE fluxes from soil and canopy. In a recent TSM application, Li et al. (2008) used Landsat data at different resolutions (see Fig. 3c), and compared satellite

[6] Two-source models are one-dimensional models which estimate the sensible and latent heat fluxes from the soil and the vegetation separately (see Kustas and Norman 1999). Two-source models have also been called two-layer models (see Kustas 1990).

retrievals with ground based flux measurements. The results illustrated good agreement at the 30 m and 120 m resolutions, but comparatively poor reproduction of latent heat flux at 960 m, highlighting the issue of sub-pixel scale heterogeneity and the difficulties in assessing remote retrievals at coarse scales.

5 Methods Using Time Rate of Change in Surface Temperature with Atmospheric Boundary Layer Models

Wetzel et al. (1984) demonstrated that the time rate of change of area-averaged surface temperature observed with geostationary satellites may be used with a one-dimensional Atmospheric Boundary Layer (ABL) model to estimate surface soil moisture and land surface fluxes. Diak (1990) improved this technique by initializing the model with air temperature, humidity and wind speed soundings and calibrating the model with T_{rad} and ABL height observations. Diak and Whipple (1993) also included horizontal and vertical advection effects in the Diak (1990) model as well as vertical motions above the ABL. The advantage of using the time rate of change approach is that offsets between the measurements of T_{rad} and T_a are cancelled out of the temperature, which reduces the need for absolute accuracy in satellite remote sensing and atmospheric correction.

A two-source time-integrated model (TSTIM) was described by Anderson et al. (1997) which was an extension of the earlier TSM model of Norman et al. (1995). Unlike TSM which uses single-time observations, TSTIM requires measurements of surface temperature at two times during the morning hours and an atmospheric temperature profile during the early daylight hours. TSTIM and its successor, the Atmosphere-Land Exchange Inverse (ALEXI) model, couple a two-source land surface model and one-dimensional ABL model. ALEXI was used by Mecikalski et al. (1999) for estimating surface λE and H fluxes over continental scales using satellite and synoptic weather data. Because the method uses time changes in T_{rad}, it is relatively insensitive to uncertainties associated with surface emissivity and atmospheric corrections.

Anderson et al. (2007a, b) recently used ALEXI to obtain surface fluxes across the continental United States. They noted that satellite overpass schedules and cloud cover may lead to frequent gaps in the output and used the ALEXI approach with a new gap-filling technique to provide time-continuous flux estimations from hourly geostationary satellite data. The gap-filling function fills flux estimates during gaps in the remote sensing record because intermittent cloud cover impacts adversely on optical remote sensing. It is based on the assumption that the fraction of potential evaporation achieved on clear days (denoted by f_{Ep}) is maintained during cloudy intervals (whilst accounting for evaporative losses from the soil) until the next clear day. On clear days f_{Ep} is mapped to an available water fraction and on cloudy days the available water fraction is inverted to estimate E_a.

The 5–10 km resolution flux estimates generated by Anderson et al. (2007a, b) with ALEXI were disaggregated to micro-meteorological scales ($\sim$100 m) with the Disaggregated ALEXI (DisALEXI) algorithm of Norman et al. (2003). It uses low-temporal, high-spatial resolution surface temperature and vegetation cover information from aircraft or satellite imagery (e.g. Landsat, ASTER, MODIS) to disaggregate ALEXI flux estimates obtained from high-temporal, low-spatial resolution (5–10 km) GOES data down to 30–300 m. Using data from the 1997 Southern Great Plains (SGP) field experiment they reported that the root-mean-square difference between remote sensing estimates and ground based measurements of latent heat fluxes was about 40 W m^{-2}. Figure 3b presents some recent results by Anderson et al. (2007c) with DisALEXI.

Norman et al. (2000) used the formulations of Anderson et al. (1997) to develop a simple dual-temperature-difference (DTD) approach which uses time rate of change in both T_{rad} and near-surface T_a. The first time is chosen when all fluxes are small and these two temperatures are close, typically just after sunrise. The second time is usually taken when the fluxes are larger and the differences between the two temperatures are near maximum i.e. around solar noon to early mid-afternoon. This approach can be used to simulate H throughout the day whilst λE is then calculated as the residual term in Eq. 1. The method reduces both the errors associated with deriving T_{rad} and with defining specific time-of-day meteorological quantities at large scales. It also eliminates the need for modelling the ABL development (see also Kustas 2000; Kustas et al. 2003a). Regional scale applications of the DTD approach resulted in RMSE values of $\sim$60 W m^{-2} when compared with tower-based λE measurements (see Kustas 2000).

6 Spatial Variability Methods

Visible, near-infrared and thermal satellite imagery has been used to develop a range of vegetation indices which have been related to land cover, crop density, biomass and other vegetation characteristics (e.g. McVicar and Jupp 1998). Vegetation indices such as the Normalized Difference Vegetation Index (NDVI), the Soil Adjusted Vegetation Index (SAVI), the Enhanced Vegetation Index (EVI) and the Simple Ratio (SR), are measures of canopy greenness which may be related to physiological processes such as transpiration and photosynthesis. The reader is referred to Glenn et al. (2007) for a detailed review. Below we explore how the observed spatial variability in T_{rad} is used with reflectance and/or vegetation index observations for evaporation estimation.

6.1 Surface Temperature, Reflectivity and Vegetation Indices

The Surface Energy BALance (SEBAL) approach (Bastiaanssen et al. 1998a, b; Bastiaanssen 2000) is used with remotely sensed surface temperature, surface reflectivity and NDVI data. The scheme represents a one-source resistance transfer scheme which derives r_s, H, λE and near-surface soil moisture. The scheme makes explicit use of the observed spatial variability in surface temperature and surface reflectance across a single cloud-free scene.

SEBAL has been designed for the regional scale and it requires few concurrent ground level observations from within the scene. K$\downarrow$ and L$\downarrow$ are computed using a constant atmospheric transmissivity, an appropriate atmospheric emissivity value and an empirical function of T_a, respectively. G is calculated as a fraction of R_n depending on T_{rad}, NDVI and α (see Bastiaanssen 2000).

SEBAL calculates instantaneous values of the sensible heat flux in three main steps. SEBAL firstly recognizes that T_{aero} is not equal to T_{rad}. It assumes that the relationship between T_{rad} and the near-surface temperature gradient (ΔT) defined as $T_{aero} - T_a$ is quasi-linear. Two extremes are identified from the image: a wet extreme where $\lambda E \gg H$ and $\Delta T = 0$, and a dry extreme where $\lambda E = 0$ and $H = R_n - G$. These extremes are used to anchor the quasi-linear relationship relating ΔT to T_{rad}, allowing ΔT to be estimated for any T_{rad} across the image.

Secondly, a scatter plot is obtained for all pixels in the entire image of broadband α values versus T_{rad}. Pixels with large E rates ($\lambda E \gg H$) are expected to have low temperature and low reflectance values, whereas areas with little or no E ($\lambda E \approx 0$ and $H \approx R_n - G$)

have high surface temperatures and generally high reflectance values. Scatter plots for large heterogeneous regions frequently show an ascending branch controlled by moisture availability and E, and a radiation-controlled descending branch where E is negligible (see for example Fig. 4 in Bastiaanssen et al. 1998b). For the ascending branch, temperatures increase with increasing α values as water availability is reduced and E becomes more limited. The descending branch indicates that increasing α will result in a decrease in surface temperature. If the radiation-controlled descending branch is well defined, r_a may be obtained from the (negative) slope of the reflectance–surface temperature relationship.

Finally, through the use of local surface roughness (z_{om}) based on the NDVI and the assumption of a fixed z_{om}/z_{oh} ratio, together with the flux profile relationships for temperature and momentum, H can be calculated for every pixel with λE as the residual term in Eq. 1. The SEBAL scheme has been used widely with satellite and aircraft data over relatively flat landscapes with and without irrigation (see Bastiaanssen et al. 1998b).

The Mapping EvapoTranspiration with high Resolution and Internalized Calibration (METRIC) method (see Tittebrand et al. 2005; and Allen et al. 2007a, b) was derived from SEBAL for use with irrigated crops. METRIC uses the crop's reference evaporation (E_{ref}) to represent fully transpiring vegetation. Extreme (cool/wet and warm/dry) pixels are identified in the given agricultural setting with the cool/wet extreme comparable to a reference crop with its evaporation rate computed from the Penman–Monteith combination equation. Evaporation from the warm/dry pixel is calculated with a soil water budget using local meteorological data. Field studies with irrigated alfalfa in Idaho showed agreement to within 5% between METRIC estimates and lysimeter observations. METRIC also uses the reference crop E to extrapolate from instantaneous E fluxes to daily rates.

Boegh et al. (1999) presented an energy balance method for estimating transpiration rates from sparse canopies. It requires spectral reflectance and surface temperature data in addition to: (i) an empirical linear relationship between the fraction of R_n absorbed by the vegetation (fR_n) and NDVI; (ii) a slope coefficient to describe the relationship between $(T_s - T_0)$ and $(T_s - T_a)$, where $T_s \approx T_{rad}$ = the observed (composite) temperature of soil and vegetation, T_0 = temperature of the mean canopy air stream computed by applying the conservation budget equation to the measured sensible heat flux and the air temperature T_a above the canopy; and (iii) the bulk leaf boundary layer conductance g_b. Model simulation (see Troufleau et al. 1997) may be used to establish a relationship between $(T_s - T_0)$ and $(T_s - T_a)$, whereas g_b values are assessed from LAI and approximate estimates of leaf size. Next, the method estimates the transpiration rate of the vegetation from the difference between the net radiation attributed to the vegetation and the sensible heat flux between leaves and the air within the canopy. The method was used in the Sahel for woodlands and agricultural crops with ground based, airborne and satellite remote sensing data and validated with sap flow and latent heat flux measurements. Agreement between remote sensing based estimates and ground based measurements of λE rates is estimated to be better than 30–40 W m^{-2}.

6.2 Surface Temperature and Reflectivity

Roerink et al. (2000) proposed the Simplified Surface Energy Balance Index (S-SEBI) approach in which the instantaneous latent heat flux (λE_i) is given by

$$\lambda E_i = \Lambda_i (R_{ni} - G_i) \tag{11}$$

where $(R_{ni} - G_i)$ is the available energy at the time of the overpass and Λ_i is the evaporative fraction defined as $\lambda E/(R_n - G)$. S-SEBI requires that the atmospheric conditions

are reasonably constant across the image and that the image contains both wet and dry areas. Λ_i is obtained from a scatter plot of observed surface temperature (T_{rad}) and Landsat TM derived broadband α values across the single scene. The scatter plot shows that all data points are contained between: (i) an upper boundary representing dry, radiation controlled conditions where all radiation is used for surface heating and α decreases with increasing surface temperature (T_H—where λE is assumed to be 0 W m^{-2}); and (ii) a lower boundary representing evaporation controlled wet conditions, where all energy is used for λE and α increases with an increase in surface temperature ($T_{\lambda E}$—where H is assumed to be 0 W m^{-2}). Λ_i for a given combination of observed α and T_{rad} is then obtained as

$$\Lambda_i = (T_H - T_{rad})/(T_H - T_{\lambda E}) \quad (12)$$

where T_{rad} is the observed surface temperature for a given pixel and T_H and $T_{\lambda E}$ are the corresponding temperatures on the upper and lower boundary, respectively. The method does not require any additional meteorological data. S-SEBI was also used with some success by Sobrino et al. (2007) with 1 km AVHRR data over the entire Iberian Peninsula.

Using the S-SEBI approach, Verstraeten et al. (2005) expressed the upper (radiation controlled) and lower (evaporation controlled) boundaries in the (T_{rad}, α) scatter plot as linear functions of the T_H and $T_{\lambda E}$ values with changing α. Validation of their estimation method was carried out with 14 EUROFLUX flux towers located in forested areas in Western Europe over an 8-month period in 1997. When the instantaneous flux estimates at the time of AVHRR overpasses for all sites and all days were compared with tower measurements an RMSE value of about 35 W m^{-2} was obtained, which was equivalent to a relative error of about 24%.

6.3 Surface Temperature and Vegetation Indices

Negative correlations existing between the NDVI and T_{rad} have been linked to evaporative cooling, although for most landscapes variations in fractional vegetation cover, soil moisture availability and meteorological conditions will cause considerable scatter in those relationships.

Hope et al. (1986) showed theoretically that r_c can be estimated from the relationship between T_{rad} and NDVI and that the slope of the NDVI/T_{rad} curve will depend on the vegetation type. Their findings were confirmed by Nemani and Running (1989) with AVHRR data over a 20 km × 25 km forested region who showed that T_{rad} had a strongly negative correlation with canopy density as expressed by NDVI and that the slope of the relationship could provide a useful parameterization of r_s.

Gillies and Carlson (1995) combined an ABL model with a SVAT model for mapping surface cover, surface soil moisture and land surface fluxes. The combined model was run for full cover with the highest known NDVI and for bare soil conditions with the lowest known NDVI in the scene for a range of soil moisture values until AVHRR observed (T_{rad}) and simulated (T_{aero}) surface temperatures matched, at which stage the actual fractional vegetation cover (f_c) and surface soil moisture were estimated. These studies led to the "triangle method" (Carlson et al. (1995a, b); Gillies et al. 1997; Carlson 2007) for estimating soil moisture status from the NDVI–T_{rad} relationship. The boundaries of this triangle constitute limiting conditions for H and λE.

Boegh et al. (1999) and McVicar and Jupp (1998) noted that the variability in T_{rad} and NDVI depends on the resolution of the remote sensing data. Higher-resolution data suggest that the variance in NDVI and T_{rad} is more strongly related to land cover type. For

incomplete cover the soil background temperature and fractional cover (f_c) can become dominant factors (Friedl and Davis 1994), whereas for lower-resolution data variance in NDVI and T_{rad} is more influenced by dominant agricultural practices and antecedent rainfall.

Jiang and Islam (2001); Venturini et al. (2004); Batra et al. (2006) elaborated on the triangle method and used an estimation methodology based on an interpolation of the Priestley–Taylor method (Priestley and Taylor 1972) using the triangular (T_{rad}, NDVI) spatial variation. The Priestley–Taylor expression for equilibrium evaporation from a wet surface under conditions of minimal advection (λE_{PT}) is given by

$$\lambda E_{PT} = \alpha_{PT}[\Delta/(\Delta + \gamma)]\,(R_n - G) \tag{13}$$

where Δ (Pa K^{-1}) is the slope of the saturated vapour pressure curve at the prevailing T_a, γ is the psychrometric constant (Pa K^{-1}) and α_{PT} is the (dimensionless) Priestley–Taylor parameter which is generally interpreted as the ratio between actual E and equilibrium E. The α_{PT} parameter is assumed to be 1.26 for wet land surface conditions.

Brutsaert (1982) pointed out that advection free conditions hardly ever occur and it may be noted here that α_{PT} values may increase to approximately 1.6–1.8 when advective conditions are experienced with strong winds and dry, hot air (Flint and Childs 1991; Castellví et al. 2001; Pereira 2004).

Global changes in air temperature, humidity, radiation and wind speed clearly also affect the α_{PT} value. This indicates that the value of α_{PT} will change in response to changes in ambient air temperature, humidity, wind speed and radiation conditions and will vary spatially; noting that Flint and Childs (1991) report α_{PT} values ranging from 0.7 to 1.6. Increases in air temperature have been reported for many parts of the world, yet perhaps less well known is that minimum air temperatures at screen level have increased more than maximum air temperatures (e.g. Vose et al. 2005). Decreases in vapour pressure deficit are occurring in many regions (e.g. Hobbins et al. 2004) as are changes in incoming solar radiation (e.g. Wild et al. 2005) and wind speed (e.g. Roderick et al. 2007). Clearly changes in the main forcing variables will impact estimates of E_{PT}, E_p and E_a.

In the Jiang and Islam (2001) approach α_{PT} is replaced by a parameter ϕ which accounts for a wide range of r_a and r_c values. The triangle method, described earlier, suggests that the warm edge of the (T_{rad}, NDVI) scatter plot represents pixels with the highest T_{rad} and with minimum evaporation from the bare soil component, while E_a can vary for different vegetation classes. Linear interpolation between the sides of the triangular distribution of T_{rad} − NDVI allows ϕ values to be derived for each pixel using the spatial context of remotely sensed T_{rad} and NDVI. The ϕ values are related to surface wetness, r_s and T_{rad}. Scene-based maximum and minimum values for ϕ are determined as $\phi_{min} = 0$ for the driest bare soil pixel and $\phi_{max} = 1.26$ for a densely vegetated, well-watered pixel. Thus the actual ϕ value for each pixel in a specified NDVI interval is obtained from the observed $(T_{rad})_{obs}$ with

$$\phi = \phi_{max}\left[(T_{rad})_{max} - (T_{rad})_{obs}\right] / \left[(T_{rad})_{max} - (T_{rad})_{min}\right] \tag{14}$$

where $(T_{rad})_{max}$ and $(T_{rad})_{min}$ are the highest and lowest surface temperatures in each narrow NDVI class which correspond with the lowest and highest evaporation rates, respectively. The evaporative fraction Λ may then be evaluated from

$$\Lambda = \phi[\Delta/(\Delta + \gamma)] \tag{15}$$

Note also the similarity with the approach of Roerink et al. (2000) described in Sect. 6.1 who used a scatter plot of T_{rad} and broadband reflectivity, rather than NDVI, and that of

McVicar and Jupp (2002) described in Sect. 7.2, who invert a two-source SEB to obtain the maximum and minimum end-members.

Wang et al. (2006) adopted the approach of Jiang and Islam (2001) but obtained better results with the spatial variation in (ΔT_{rad}, NDVI), where ΔT_{rad} is the day–night difference in T_{rad} as obtained from MODIS imagery. However, their method still requires estimation or measurement of net radiation (R_n) and soil heat flux (G) to convert Λ into E.

In a later paper Jiang and Islam (2003) adopted fractional vegetative cover (f_c) as a more suitable generalized vegetation index calculated from the normalized NDVI* with

$$f_c = (\mathrm{NDVI}^*)^2 \tag{16}$$

where

$$\mathrm{NDVI}^* = (\mathrm{NDVI} - \mathrm{NDVI}_{min})/(\mathrm{NDVI}_{max} - \mathrm{NDVI}_{min}) \tag{17}$$

The difference between surface and air temperature ($\Delta T = T_{rad} - T_a$) was considered more representative of the sensible heat flux H than T_{rad} and a transformed parameter set (f_c, ΔT) was used. It was assumed that within a certain f_c class the evaporative fraction $\Lambda = \lambda E/(R_n - G)$ is linearly related to ΔT. Interpretation of the triangle space of (f_c, ΔT) shows that the evaporative fraction may be estimated from f_c and ΔT for a given set of ΔT_{max}, ΔT_e and β, where ΔT_e is ΔT_{max} at $f_c = 1$ and β is a stress factor. Using AVHRR data they show that this simple interpretation scheme yielded comparable, or better, results than obtained with the aerodynamic resistance-energy balance method represented by Eq. 6 which includes atmospheric stability corrections and employs an iterative procedure to obtain the most appropriate kB^{-1} value.

A procedure similar to that outlined by Jiang and Islam (2001) was reported by Schüttemeyer et al. (2007) who estimated actual evaporation from semi-arid terrain in Ghana by multiplying potential evaporation, computed with the Makkink equation from METEOSAT-7 near-surface temperature and radiation data, with AVHRR-derived fractional green cover data in an approach originally proposed by Choudhury and De Bruin (1995).

Many techniques for estimating E from remote sensing data require ground based observations which are often not available. Nishida et al. (2003a) described an operational method which estimates the evaporative fraction Λ from optical satellite remote sensing data only. The method is tailored to the MODIS/Aqua sensor although the approach was developed with NOAA-AVHRR data. The algorithm uses a two-source model and the evaporative fraction of vegetation (Λ_{veg}) is estimated using the complementary relationship between actual and potential E expressed by Eq. 23. The evaporative fraction of bare soil (Λ_{soil}) is estimated with the triangular relationship between NDVI and T_s as described by Gillies et al. (1997). The NDVI–T_s scatter diagram allows estimation of maximum soil temperature $(T_{soil})_{max}$ (for bare soil at $NDVI_{min}$), actual T_{soil} at NDVI and minimum soil temperature $(T_{soil})_{min}$ at $NDVI_{max}$ which is considered to be close to vegetation temperature T_{veg} and air temperature T_a. The method provides instantaneous flux data or evaporative fraction values which are assumed to be constant throughout the day. The technique has been applied with bi-weekly 1 km AVHRR data, and validated against measurement from 13 AmeriFlux sites located across the continental United States showing a standard error in Λ of ± 0.17 and an r^2 of 0.71. The method assumes a linear relationship between NDVI and the fractional vegetation cover (Lu et al. 2003). Use of MODIS/Aqua data rather than AVHRR data should improve estimation of α, T_{rad} and vegetation indices.

A satellite-derived index of land surface evaporation based on the above algorithm for use with MODIS/Aqua data is presented in a paper by Nishida et al. (2003b) who describe the advantages of using MODIS/Aqua as: (i) improved spectral and radiometric resolution for deriving surface temperatures and vegetation indices; (ii) the availability of atmospheric temperature and vapour pressure profile data as well as the possibility of using AMSR-E soil moisture data; and (iii) increased frequency of evaporative fraction and evaporation estimates when compared with other sensors.

6.4 Empirical Vegetation Index Methods

Glenn et al. (2007) reviewed studies correlating vegetation indices and evaporation. They note that for E estimation from agricultural crops the most direct application is to substitute the vegetation indices for crop coefficients which are defined as the ratio between actual crop water use and reference crop E (Allen et al. 1998) for the given set of local meteorological conditions. For agricultural crops and natural ecosystems they reported linear correlations between E and NDVI with r^2 values of about 0.81. In natural ecosystems the vegetation indices may be used for up-scaling from ground based E measurements based on flux towers to larger spatial domains. Glenn et al. (2007) also noted the lack of linear relationships between remotely sensed vegetation indices and canopy properties such as LAI and f_c, and suggested that vegetation indices should be used directly rather than attempting to convert them first into LAI or f_c estimates (see also Lu et al. 2003).

The relationship between NDVI and actual evaporation was also clearly illustrated by Loukas et al. (2005) who successfully used linear relationships between monthly composites of NDVI and actual E simulated with a water balance model to estimate basin-wide actual evaporation in four watersheds in Central Thessaly, Greece, ranging from 134 and 394 km^2.

Nagler et al. (2005a, b) estimated evaporation from riparian vegetation with simple regression equations based on the MODIS derived Enhanced Vegetation Index (EVI) (see Huete et al. 2002) and maximum daily air temperature. Correlations with data obtained with flux towers over riparian vegetation along three major river systems in the southwestern United States over 2000–2004 showed that daily E could be simulated with an r^2 value of 0.76. More recently Nagler et al. (2007) correlated 16-day MODIS EVI values with E observations obtained with flux towers in semi-arid rangeland in Arizona. A simple multiple linear regression fit of E to EVI and precipitation resulted in $r^2 = 0.74$.

Eight sites throughout the Southern Great Plains in the US with Bowen Ratio E observations, net radiation and soil heat flux measurements, observations of relevant meteorological parameters and coincident MODIS satellite data were used for a three-year period by Wang et al. (2007) to investigate correlations between E and the air and surface temperatures, vegetation indices, net radiation and soil moisture. Using daytime averages, net radiation, temperatures and vegetation indices are the top three variables correlated with E_a. There was a near-linear relationship between net radiation at the surface and E_a, so R_n values were used to normalize E_a which was expressed as a linear combination of NDVI and either daytime maximum T_a or T_{rad}. The authors parameterized the normalized actual evaporation $E_n = E_a/R_n$ as a linear function of vegetation index and air or surface temperature. For daytime averages the regression of E_n on the combination of EVI and maximum air temperature $(T_a)_m$ showed that E could be estimated with an r^2 value of 0.83 and a RMSE of about 30 W m^{-2}, which was about 20% of the average E across all sites and all three years. Sensitivity analysis showed for EVI = 0.35, $R_n = 350$ W m^{-2} and $T_a = 25°C$ that the relative error in E resulting from a 4 K error in T_a was found to be

3.8%. Similar sensitivities were observed for EVI and R_n: the relative error in E from an error of 0.04 in EVI was 7.8% and the relative error caused by an error of 20 W m^{-2} in R_n was 5.8%. The authors noted that these sensitivities to errors in T_a, EVI and R_n are much less than those obtained for methods using surface–air temperature gradients such as TSM (see Timmermans et al. 2007).

The above method was validated against an independent data set based on flux tower eddy covariance measurements at 6 sites, comprising grassland, cropping and forests. Correlation between four years of 16-day averaged estimates based on net radiation, EVI and maximum air temperature and measurements of E_a yielded r^2 values of 0.71–0.90, RMSE values of 24–39 W m^{-2}, and relative errors of 29–48%. It is also noted that part of the errors encountered are associated with uncertainty in the eddy covariance method. The accuracy achieved with this simple regression method is comparable if not better than that achieved with far more complex methods described elsewhere in this paper and certainly meets the required E retrieval accuracy of about 50 Wm^{-2} suggested by Seguin et al. (1999).

7 Estimating Evaporation with Surface Temperatures and Meteorological Data

7.1 Crop Water Stress and Water Deficit Indices

Numerous studies have investigated since the early 1960s how foliage temperature may be used to estimate crop water stress. Kustas et al. (2003a) distinguished between methods for estimating crop water stress based on: (i) canopy-air temperature differences ($T_c - T_a$); (ii) comparison with foliage temperatures in a well-watered field; and (iii) variability of foliage temperatures within a field.

The widely used Crop Water Stress Index (CWSI) method (see Jackson et al. 1981) is based on observed canopy-air temperature differences. When a crop with full cover has adequate water it will transpire at the potential rate for that crop. The actual transpiration (i.e. evaporation) rate (E_a, mm h^{-1}) will fall below the potential rate (E_p, mm h^{-1}) when water becomes limiting. The ratio (E_a/E_p) is therefore an index of soil moisture availability. The ratio E_a/E_p will range from 1 (ample water; canopy resistance R_c is lowered to its potential value R_{cp} at potential transpiration E_p) to 0 (no available water, R_c becomes infinitely large). The CWSI ranges from 0 (no stress) to 1 (maximum stress) and has been defined as

$$\mathrm{CWSI} = 1 - \left(E_a/E_p\right) \tag{18}$$

Jackson et al. (1981) expresses ($T_c - T_a$) for a closed canopy as a function of the available energy ($R_n - G$), vapour pressure deficit ($e_a^* - e_a$), r_a and r_c. Hence CWSI may be expressed in terms of differences between canopy temperature and air temperature (see Choudhury 1983) as

$$\mathrm{CWSI} = \left[(T_c - T_a) - (T_c - T_a)_{\min}\right] / \left[(T_c - T_a)_{\max} - (T_c - T_a)_{\min}\right] \tag{19}$$

where the subscripts min and max refer to unstressed conditions (i.e. maximum transpiration) and conditions of maximum stress (i.e. no transpiration).

Choudhury (1989) defined CSWI in terms of foliage temperatures as

$$\mathrm{CWSI} = \left(T_v - T_v^o / T_v^{\max} - T_v^o\right) \tag{20}$$

where $T_v{}^o$ and T_v are, respectively, the infrared foliage temperature of well-watered and water-stressed canopies, and $T_v{}^{max}$ is the maximum attainable foliage temperature under

the prevailing atmospheric conditions with a non-transpiring crop. CWSI may also be described with a resistance expression (see also Kustas et al. 2003a).

$$\mathrm{CWSI} = 1 - \left(E_a/E_p\right) = \left[1 + \left(r_{cp}/r_a\right)\right]/[1 + (r_c/r_a)] \tag{21}$$

where all symbols retain their previous meaning.

The CWSI concept was originally developed for complete canopy conditions so that the observed surface temperatures may be assumed to be equal to the canopy temperatures; modifications are needed to use this approach for incomplete fractional cover (f_c).

Moran et al. (1994) used the Penman–Monteith equation with known values of R_n, e_a and u to define the theoretical boundaries in the two-dimensional Soil Adjusted Vegetation Index (SAVI)/($T_{rad} - T_a$) space. The boundaries define a trapezoid and local E rates were obtained from the location of local SAVI/($T_{rad} - T_a$) measurements within the date- and time-specific trapezoid. This "trapezoid method" can thus be used for estimating a Water Deficit Index (WDI) as well as the actual E_a for each pixel with uniform or non-uniform land cover if representative ground information is available to calculate the land surface fluxes at each of the vertices. It has been postulated that the narrow upper segment of the trapezoid collapses to a single vertex based on land surface/pixel size interactions (McVicar and Jupp 1998). This narrowing at the top of the trapezoid is most likely due to the fact that in natural ecosystems landscapes with full vegetation cover are usually not water stressed. Lambin and Ehrlich (1996) used an approach similar to that of Moran et al. (1994) for heterogeneous landscapes.

Boulet et al. (2007) used time sequences of surface temperature over wheat (with LAI values ranging between 0 and a maximum of 4) and sparse grass (with LAI values < 1) to show that the difference between the observed (actual) surface temperature (T_s) and the surface temperature for unstressed (potential) conditions (T_{sp}) may be used to estimate a stress factor S which is defined as $S = 1 - (\lambda E/\lambda E_p)$. Here ($T_s - T_{sp}$) approximates the foliage temperature difference ($T_v - T_v^o$) in Eq. 20 for full cover and S approximates CWSI in Eq. 18. Boegh et al. (2002) express the control of the surface resistance (r_s) on the latent heat flux through the Surface Control Coefficient (SCC) which is defined as $\mathrm{SCC} = 1 - \Omega$ where Ω is the decoupling coefficient of Jarvis and McNaughton (1986). This decoupling coefficient expresses the degree of coupling between atmosphere and land surface as a function of the relative importance of atmospheric and surface resistances (see Overgaard et al. 2006).

7.2 Normalised Difference Temperature Index

The various methods described in Sect. 6 (SEBAL, S-SEBI and WDI) are limited by the fact that each condition, i.e. very wet and very dry, fully vegetated and completely bare surfaces is not always present on a given image. McVicar and Jupp (2002) developed the Normalised Difference Temperature Index (NDTI) to overcome this limitation. NDTI defines the temperatures for very dry and very wet conditions by inverting a two-source SEB model and places the observed T_s values in an envelope defined by the modeled maximum and minimum temperatures. Thus

$$\mathrm{NDTI} = (T\infty - T_s)/(T\infty - T_0) \tag{22}$$

where the $T\infty$ and T_0 values are calculated by setting the appropriate r_s values to ∞ s m^{-1} and 0 s m^{-1} respectively. These two resistances represent conditions of no

evaporation and potential E, respectively. The NDTI represents an index of moisture availability and provides an estimate of the relative evaporation $\Lambda_r = E_a/E_p$. The NDTI method can be considered as a specific time-of-day version of the CWSI, though the requirements for wet and dry pixels in the same image are avoided. The inversion of the REBM is conducted at the time of the overpass, and to increase the number of locations available for this, input data are estimated from meteorological stations with daily time-step data (McVicar and Jupp 1999). Next, the NDTI values calculated at the isolated stations are spatially interpolated (in a 'calculate-then-interpolate' approach) using remotely sensed and meteorological covariates (McVicar and Jupp 2002). Estimates of E_a may be obtained by multiplying the NDTI by some estimate of E_p (see for example McVicar et al. 2007a).

Nearly 9000 single-pass afternoon AVHRR images for south-east Australia have been processed using the NDTI approach since mid-1992 (McVicar et al. 2007b). In this area, with just over 2 million terrestrial 0.01° AVHRR pixels, there are only 217 meteorological stations (recording daily maximum and minimum air temperature and daily precipitation). The NDTI series shown in Fig. 4a is dominated by relatively higher values of relative evaporation along the eastern sea-board. Generally higher values of the relative evaporation associated with summer rains are seen in the north, while in the south one can observe the increase in Λ_r associated with winter rain that is utilized by the dryland broad-acre farms. The series of E_p generally follows the seasonal trends, though it is slightly modulated by the controls of topography on R_n and of surface elevation on T_a (e.g. McVicar et al. 2007a) in the mountainous regions of south-east Australia. Finally, the series of E_a (coupling the high spatial variability of the NDTI with the climatologically driven surfaces of E_p) shows distinct temporal and spatial trends in E_a.

To highlight the spatial detail, Fig. 4b focuses on the Coleambally Irrigation Area (CIA), a rice-based irrigation system (where rice is flood irrigated), with other summer crops (that are furrow irrigated) including corn, soybeans and sorghum (Van Niel and McVicar 2004b; Van Niel et al. 2003), with surrounding dryland farms. There are a number of drains west of the irrigation area used to remove excess water from the region. Features to note include: (i) the lack of spatial variance in the E_p data contrasting that present in the NDTI and E_a data; (ii) high summer NDTI and E_a values in the irrigation area; (iii) drain outflow being captured to the west of the irrigation area in summer; and (iv) relatively high NDTI values in winter of both irrigation and surrounding dryland farms (due to widespread precipitation) so irrigation demand is lower as landholders attempt to utilize residual soil moisture after successfully growing summer crops (Van Niel and McVicar 2003).

Figure 5a–c show fortnightly data extracted for an 80 km long transect running west–east through the centre of Fig. 4b (also running through the CIA) for NDTI, E_p and E_a, respectively. In each figure the x-axis is the distance along this transect and the y-axis is time through the year. These figures highlight patterns of the three distinctive regions of the CIA-subset, being: (i) west of CIA where the impact of the CIA drain is seen (0–30 km along the transect); (ii) the CIA proper (30–58 km); and (iii) dryland agriculture east of the CIA (58–80 km). Figure 5a–c illustrate the same seasonal differences as shown in Fig. 4b. In addition, they also reveal some finer-scale features. For example, NDTI and E_a increase west of the CIA in the second fortnight of January, yet it takes another fortnight for the vegetation to respond, as detected by an increase in the NDVI (McVicar et al. 2007b). In the second fortnight of January direct evaporation from the soil surface would have been high before the vegetation responded. Also in the early part

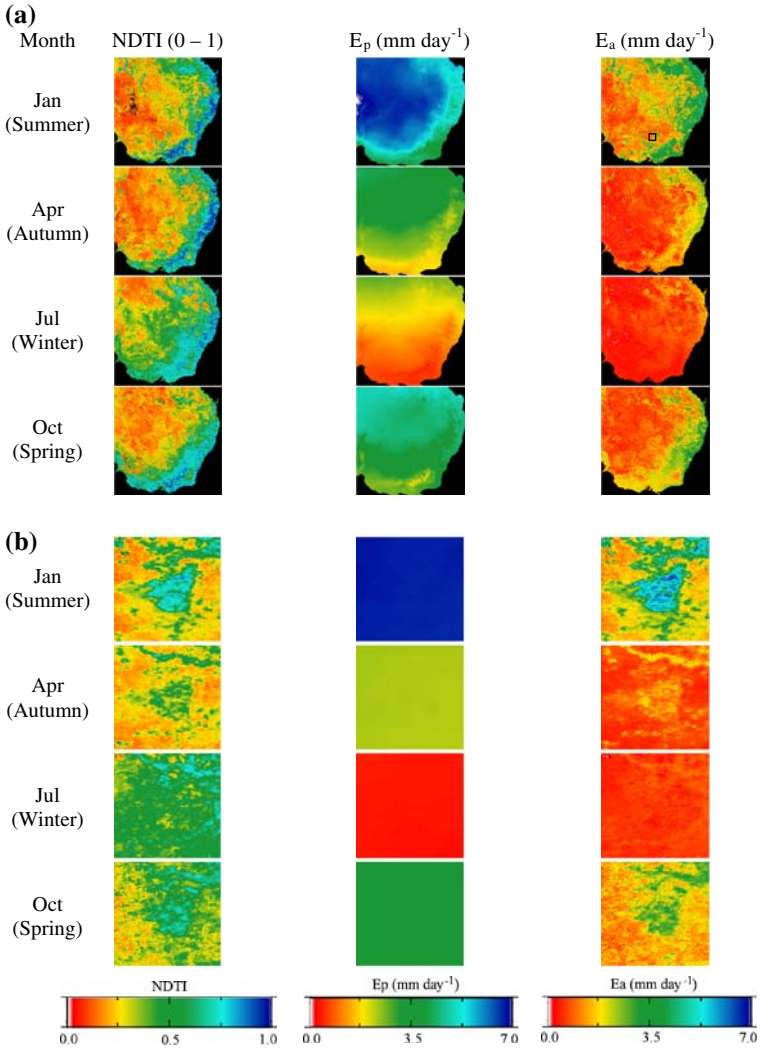

Fig. 4 Selected monthly surfaces of NDTI, E_p and E_a for 2001 for: (**a**) all of south-east Australia; and (**b**) an 80-km subset focusing on the Coleambally Irrigation Area (CIA). In both the central months of the four seasons are shown, and the location of the CIA is provided on the summer E_a data in (**a**). The NDTI is a monthly composite and for E_p and E_a monthly daily averages are shown

of the summer growing season (i.e. October and November) there is considerable evaporation from the flooded rice paddocks prior to canopy closure; it is unlikely that this would be detected using conductance measures derived from remote sensing based LAI data as implemented by Cleugh et al. (2007). Figure 5d–f are standard time series plots for individual pixels.

The accurate estimation of E_a from intensive irrigation areas (such as the CIA) is an important feature of accurate water accounting systems that are currently being developed in many countries as competition for water resources increases. A review of the application of remote sensing technology to assist rice-based irrigation system management is

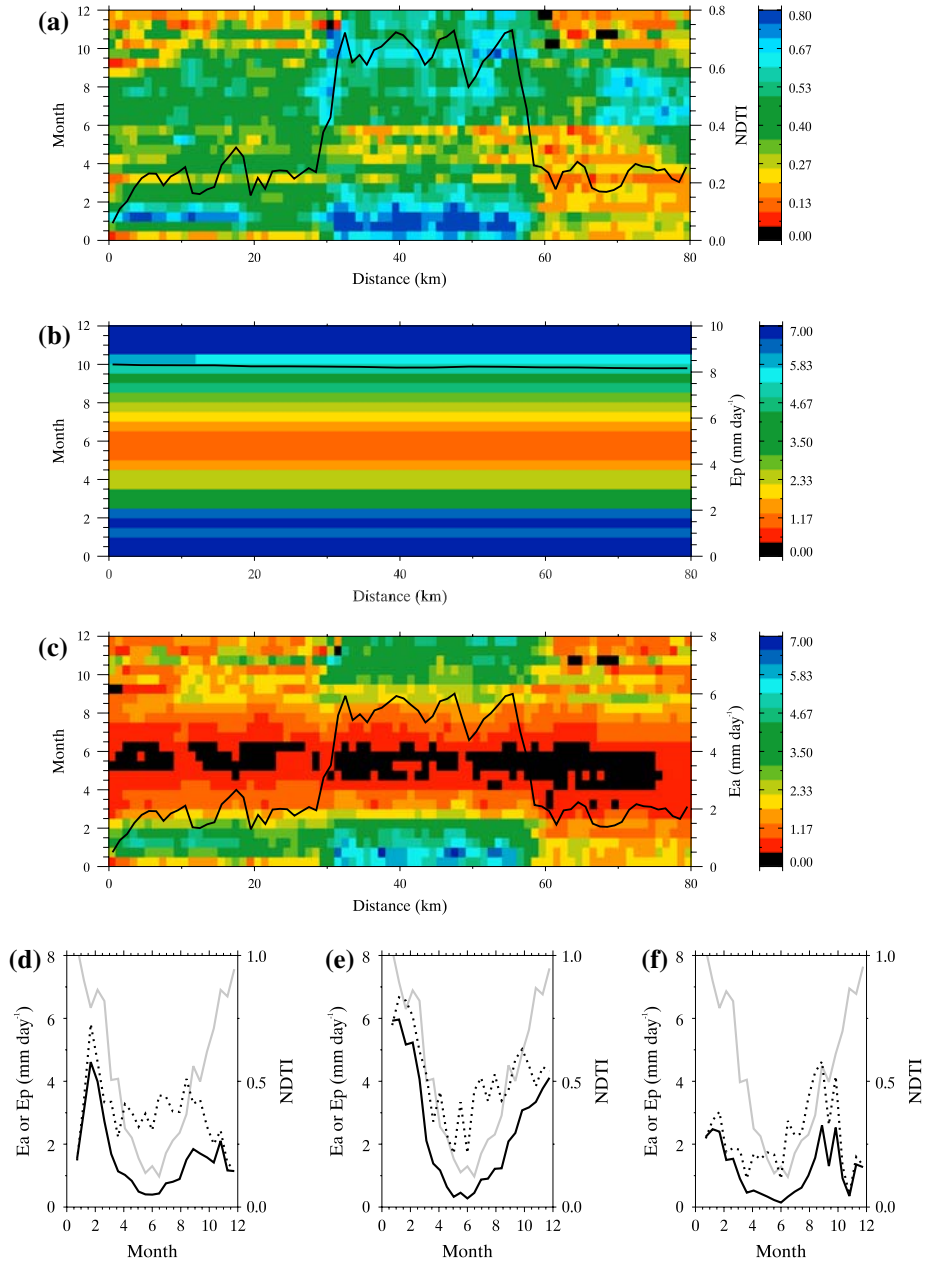

Fig. 5 Fortnightly time series plot from 2001 for an 80 km transect located across the Coleambally Irrigation area of (**a**) NDTI; (**b**) E_p; and (**c**) E_a. The black line in (**a**), (**b**) and (**c**) is the profile of the first fortnight. Per pixel time series are shown for pixels located at (**d**) 15 km, (**e**) 40 km; and (**f**) 65 km, respectively, with the dashed line being the NDTI, the grey line being E_p and the black line being E_a. The NDTI is a fortnightly composite and fortnightly daily averages for E_p and E_a are shown

provided by Van Niel and McVicar (2004a); the CIA example complements that work, by highlighting how regional remotely sensed data can be used to monitor irrigation system performance.

7.3 Methods Based on the Complementary Approach

The complementarity relationship of Bouchet (1963) states that, as the land surface dries, the decrease in actual E is accompanied by an equal but opposite change in the potential E. This is expressed in

$$E_p + E_a = E_w \tag{23}$$

where E_p is the potential evaporation that would occur under prevailing atmospheric and energy conditions if evaporation was not water limited, E_a is the actual evaporation and E_w is the evaporation of an extended wet surface when $E_a = E_p = E_w$. Granger (1989) derived definitions for both E_p and E_w from the energy balance and mass transfer equations and expressed both in terms of vapour pressure gradients. Granger then introduced the following expression for an alternative complementary approach

$$E_a + E_p(\gamma/\Delta) = E_w[1 + (\gamma/\Delta)] \tag{24}$$

where all symbols retain their previous meaning.

Venturini et al. (2008) used Eq. 24 with estimates of the wet environment evaporation (E_w) obtained with the Priestley–Taylor equation given by Eq. 13. The relative evaporation ratio $\Lambda_r = E_a/E_p$ is then approximated with

$$\Lambda_r = (T_u - T_d)/(T_s - T_d) \tag{25}$$

where T_d is the dewpoint temperature; T_s is the observed surface temperature with $T_s \approx T_{rad}$; and T_u is the (unknown) temperature reached by the surface if it is brought to saturation without changing the actual surface water vapour pressure ($e_s = e_u^*$). It may be generally assumed that $e_s^* \geq e_s \geq e_a$ so that $T_d \leq T_u \leq T_s$. Venturini et al. (2008) show how T_u may be estimated from the saturation vapour pressure curve with the approximation

$$T_u = [(e_s^* - e_a) - \Delta_1 T_s + \Delta_2 T_d]/(\Delta_2 - \Delta_1) \tag{26}$$

where Δ_2 and Δ_1 represent the slopes of the tangent to the saturation vapour pressure curves at T_d and T_s, respectively. Once T_u has been estimated, Λ_r may be calculated with Eq. 25. Finally, if E_w is computed with Eq. 13 and with $E_p = E/\Lambda_r$, one may calculate the actual evaporation for any surface from

$$E_a = \alpha_{PT}[(\Lambda_r \cdot \Delta)/(\Lambda_r \cdot \Delta + \gamma)](R_n - G) \tag{27}$$

where α_{PT} is the Priestley–Taylor parameter, assumed to be equal to 1.26. In their study over the Southern Great Plains, Venturini et al. (2008) used the1 km MOD11 product as the source of surface temperature data and obtained air and dew point temperature profiles from MOD07. The instantaneous E_a values generated with Eq. 27 were integrated to more meaningful time scales, such as daily totals, using methods such as described by Batra et al. (2006). Daily E_a totals obtained on 7 clear sky days in 2003 were compared with flux measurements obtained at 15 Energy Balance Bowen Ratio stations distributed across the $3° \times 3°$ region. Results indicate that E_a may be obtained with an estimation error of $\pm 15\%$.

8 Use of Remotely Sensed Surface Temperature Data with Land Surface Models

8.1 Calibration of Land Surface Models; Parameter Optimization

Since the 1980s a wide range of Land Surface Models (LSMs) and Soil–Vegetation–Atmosphere (SVAT) models have been developed to estimate heat and mass transfer at the land surface. LSMs contain physical descriptions of the transfer in the soil–vegetation–atmosphere continuum, and with proper initial and boundary conditions provide *continuous* simulations when driven by weather and radiation data. As Overgaard et al. (2006) discussed, energy-based LSMs are of particular interest because these approaches allow for a strong link to remote sensing applications.

One limitation of LSMs is that they often require many input parameters related to vegetation and soil characteristics which are not readily available for landscapes or regions. Another concern is that the models may be used to address questions outside the area of application for which they have been developed.

The principal objective of model calibration is to improve estimations and to identify likely parameter values for future modelling applications. Calibration involves adjusting the model parameters in order to closely match model output to some observed system behavior. This process becomes increasingly complicated when the spatial extent is increased from the local to regional scale and beyond, and more effective methods are required for calibrating regional-scale LSMs and developing appropriate land surface parameterizations.

Franks and Beven (1997, 1999) employed a SVAT model (TOPUP) to explore a new stochastic approach to obtain improved representation of the spatial variability of land surface fluxes, through the combination of Monte Carlo simulation of multiple model realizations and spatial fluxes derived from Landsat TM. McCabe et al. (2005a) applied the Franks and Beven methodology for parameter optimization and for spatial disaggregation of modeled surface fluxes across a landscape using a time series of AVHRR derived land surface temperatures. Through model calibration by minimizing differences of the modeled T_{aero} and the observed T_{rad}, they obtained insight into both: (i) the evaporative patterns across a 275 km^2 catchment; and (ii) the temporal development of the surface resistance (r_s) over 51 days.

Crow et al. (2003) used infrared surface temperatures from GOES, coupled with streamflow observations, to improve estimates of monthly evaporation derived from the VIC land surface model over the Southern Great Plains in the United States. Utilizing a multi-objective model calibration approach (Franks and Beven 1997; Gupta et al. 1998; Vrugt et al. 2003) they were able to reduce errors in model estimates of monthly evaporation by up to 20% relative to single-objective model calibration against streamflow alone.

Generally though, efforts to utilize the spatially distributed nature of remote sensing data as a calibration source have been limited, with the focus over the last decade placed on data assimilation approaches to update model states, rather than inform the actual model structure. Traditionally, observed streamflow has been the single variable through which calibration of LSMs has progressed. This may be sufficient in simple rainfall-runoff processes, but in detailed land surface modelling efforts which attempt to reproduce distributed output on diverse variables and characterize system states in a dynamic manner, it is completely inadequate. Efforts to provide more multi-objective based assessment frameworks are required to enable improved representation of the Earth system using our current modelling capacity. Remote sensing approaches provide the only means of effectively addressing this.

8.2 Data Assimilation in Land Surface Models

Data assimilation is the incorporation of observations into a numerical model(s) with the purpose of providing the model with the best estimate of the current state of a system. Thus the numerical model must have the capacity to closely represent dynamic changes occurring in the system, and accept the on-line insertion (assimilation) of new observational data distributed heterogeneously in time and space.

There are two types of data assimilation: (i) sequential assimilation which involves correcting state variables (e.g. temperature, soil moisture) in the model whenever remote sensing data are available; and (ii) variational assimilation when unknown model parameters are changed using data sets obtained over time windows of days to weeks.

Remotely sensed land surface temperatures have been assimilated at point scales into various schemes for estimating land surface fluxes by comparing simulated and observed temperatures and adjusting either a state variable (e.g. soil moisture) or model parameters in the land surface process model. Such use of remote sensing data has highlighted problems of using spatial remote sensing data with spatial resolutions of tens or hundreds of kilometres with point-scale SVAT models and has led to the search for "effective" land surface parameters (e.g. Courault et al. 2005; Boulet et al. 1999).

The use of remotely sensed T_{rad} data for updating model parameters has been described by numerous authors including Taconet et al. (1986); Braden and Blanke (1993); Kustas et al. (1994a, b) and Ottlé and Vidal-Madjar (1994). These authors have shown the feasibility of simulating the diurnal course of land surface fluxes with a SVAT model and periodically updating a key model parameter such as canopy resistance using remotely sensed surface temperature data. For example, Olioso et al. (2002a) described the successful assimilation of remote sensing data with a one-dimensional version of the land surface parameterization scheme of Noilhan and Mahfouf (1996). Van den Hurk et al. (1997) described how E maps derived from satellite data with the SEBAL approach (see Sect. 6.1) may be used to develop soil moisture fields for use in the initialization of an operational NWP model.

Significant progress has been made in recent years in estimating surface fluxes from thermal imagery sequences through the use of temporal temperature changes, which reduce the need for absolute accuracy in satellite measurements, atmospheric corrections and precise land surface emissivity evaluation (see also Sect. 5). For example, Jones et al. (1998a, b) and Suggs et al. (1999) have assimilated surface heating rates derived from temporal changes in GOES surface temperature as proxy surface wetness measures in a regional atmospheric model and a mesoscale numerical weather prediction model, respectively.

Caparrini et al. (2003) used an adjoint-state variational data assimilation approach (see Sun 1994) to map surface energy balance components at 1.1 km resolution for an 18-day period across an 8230 km^2 basin using sequences of multi-satellite remotely sensed land surface temperature measurements and data from surface climate stations. Variational approaches are based on the formulation of an inverse (adjoint) physical constraint derived from the forecast (forward) model. The assimilation problem is then redefined as an iterative process aiming at minimizing the gap between observed and predicted states. The two most critical parameters were found to be: (i) a dimensionless bulk heat transfer coefficient C_{BN} which captures how the landscape impacts on near-surface turbulence under neutral conditions; and (ii) the evaporative fraction (Λ) which reflects surface control on the relative magnitude of latent and sensible heat fluxes.

In their study, Caperrini et al. (2003) used a forward force-restore model (see Bhumralkar 1975) for predicting the time evolution of the land surface temperature as a function of R_n, H and λE, thermal inertia and deep ground temperature. Their assimilation scheme compared remotely sensed land surface temperature with predictions based on the forward model. The scheme then merged the two estimates by minimizing the squared difference between the measured and the predicted states over the entire assimilation period. The assimilation of observed land surface temperatures provided time-invariant values of C_{BN} across the basin as well as daily values of the evaporative fraction Λ. The study demonstrated the capability to map latent and sensible heat fluxes at half-hourly time steps from remotely sensed land surface temperatures and surface meteorological data. The authors concluded that longer assimilation windows should be considered so that predictive relations may be established between the critical C_{BN} and Λ parameters and local atmospheric forcing and landscape factors.

In a later paper Caparrini et al. (2004) presented results of model tests using forcing data and independent validation data from the First ISLSCP Field Experiment (FIFE). They explored the use of remotely sensed land surface temperatures for regional E mapping by under-sampling the FIFE ground based surface temperature measurements and by using only five land surface temperature measurements per day which corresponded to the number of overpassses of existing orbiting satellites. Comparisons with measured H and λE fluxes yielded RMSE values of 78 and 50 W m^{-2}, respectively, when using five T_{rad} observations, while such errors were 76 and 48 W m^{-2} when all half-hourly T_{rad} values were used.

While there has been some progress employing data assimilation approaches to improve model predictions, particularly in regards to soil moisture investigations (Houser et al. 1998; Walker and Houser 2001; Pan and Wood 2006), surface flux assimilation presents a more difficult problem (see Pan et al. 2008). One of the key limitations of land surface modelling approaches is that they, by construct, *force* energy and water balance closure. While this is certainly a desirable outcome, the usual means of accounting for water surplus is by routing to the soil moisture store and increasing the efficiency of E through parameter calibration. Such water budget constraints routinely lead to over-estimation of E (Haddeland et al. 2006), even if maintaining good agreement to runoff estimates.

9 Discussion

9.1 Limitations of Estimates Derived from Thermal Imagery

This section provides an overview of the limitations of the methods described in earlier sections and identifies issues which cause uncertainty in E estimation.

Errors in the land surface temperature. There is considerable uncertainty about the accuracy of T_{rad} observations due to the roles of atmospheric factors and surface emissivity, as well as view angle effects. A number of direct retrieval algorithms (which use atmospheric soundings combined with radiative transfer models) and indirect retrieval algorithms (which only use satellite observations) have been proposed to correct for atmospheric effects and to obtain the brightness temperature, which is the temperature of a black body that would have the same radiance as that observed by the radiometer (see Norman and Becker 1995). Emissivity information is needed in order to estimate the radiative temperature of the land surface.

All estimation methods using land surface temperature and air temperature are affected by errors in the estimation or measurements of those temperatures. Timmermans et al. (2007) recently conducted an intercomparison of the TSM model (see Sect. 4.2) and the SEBAL model (see Sect. 6.1). Sensitivity analysis showed that uncertainty in surface temperature had a significant impact on sensible heat flux (H) estimation. It was shown that a 3 K deviation in surface temperature yielded H deviations with TSM of up to 75%. A similar deviation in the difference between surface and air temperature with SEBAL led to H deviations of up to 45%.

Few models deal explicitly with the inequality between T_{rad} and T_{aero}. The difference between these two temperatures depends on many factors, including vegetation type and fractional cover f_c as well as the view angle θ.

Uncertainty in observations of T_{rad} and T_{air} may be reduced by using the temporal variation in temperature (see Sect. 5) or by using the spatial variation in T_{rad} (as described in Sect. 6), thus reducing the need for absolute accuracy in satellite observations of T_{rad}. This has been done through the use of image-based calibration procedures (e.g. Bastiaanssen et al. 1998a) or by introducing an excess resistance (r_{ex}) (see Kustas et al. 2003a). However, the estimation of r_{ex} as a function of z_{om} and z_{oh} is uncertain as it requires assumptions about the constancy of the ratio between the two roughness lengths, as well as information about wind profile and atmospheric stability.

Another serious limitation of several spatial variability methods is that the highest and lowest surface temperatures observed in the one scene are assumed to represent very dry and very wet pixels and that those extreme values are a necessary component of the estimation procedure although there is no certainty that those conditions are actually present in the scene.

Errors in estimates of the available energy. The available energy ($R_n - G$) may be obtained from ground based point observations of R_n and G, but would then lack spatial representativeness. Estimation of R_n requires observations of $K\downarrow$, α, LAI, emissivity of land surface and atmosphere, and T_{rad}. Note that such estimation of R_n brings together errors in the estimation of both short and long-wave components. There is also the need for sub-models to estimate G, for example as function of NDVI. For daily models G is often ignored. An alternative approach is to assume that G is a constant fraction of R_n (e.g. $G = 0.1R_n$), but this ignores diurnal variation as well as the fact that there is a phase difference between the diurnal cycles of R_n and G.

Other data requirements. The models described in this paper generally show a demand for ground based meteorological data such as air temperature and wind speed. The time and location of air temperature (T_{air}) observations, as well as their spatial representativeness, are critical when the method depends on computing ($T_{aero} - T_{air}$). Wind speed and aerodynamic surface characteristics pose a major challenge. Estimates of the aerodynamic resistance r_a require stability corrections as well as suitable values for roughness lengths z_{om} and z_{oh} and zero displacement level d, although some authors (e.g. Boegh et al. 2002) have developed iterative techniques to estimate r_a which do not require estimates of surface parameters or adjusted kB^{-1} values.

Models are used (e.g. Diak 1990) which integrate the planetary boundary layer (PBL) and simulate the temporal and vertical evolution of temperature and wind speed. Such models require radiosonde data or output from global circulation models (GCMs) to initialize the modelling. Other studies use air temperature at greater heights (e.g. 50 m above the ground rather than the usual screen reference height) to achieve greater spatial representativeness.

Incomplete vegetation cover. Two-source models have been developed to address incomplete vegetation cover. Such models require parameterizations for the partitioning of the computed surface temperature between soil and vegetation, for the turbulent exchange

of heat and mass between soil and atmosphere and between vegetation and atmosphere. Various resistance networks have been proposed to represent the coupling/decoupling of energy/mass exchanges in the soil–vegetation–atmosphere continuum. Two-source models also require assumptions about solar transmittance, extinction coefficients and canopy emissivity in order to estimate R_n profiles in the canopy.

Limitations of spatial variability methods. The most serious limitation of spatial variability methods such as the triangle method is that a large number of pixels are required over the area of interest with a wide range of soil wetness and fractional vegetation cover. There is also some subjectivity involved in determining the so-called warm edge and the vegetation limits of bare soil and full cover. Identification is more easily achieved with high resolution images or with images displaying a sufficiently wide range in surface wetness conditions and land cover conditions.

Limitations of empirical vegetation index models. Wang et al. (2007) indicated that use of their empirical vegetation index model should be restricted to regions where net radiation is a major controlling factor and where large scale advection is not important. Glenn et al. (2007) lists a number of other empirical approaches which have different dominant controls. They also point out that empirical vegetation index methods may be useful at time scales of weeks to years but are unable to capture E at time scales of days or shorter, as required in irrigation applications. It is also noted that "such time series studies may be confounded by spurious autocorrelations if E and vegetation index independently follow the same seasonal trend" (see Glenn et al. 2007, p. 152).

Limitations of process based models. The land surface models described in Sect. 8 vary widely in their complexity. In recent decades, these models have become very complex with large numbers of parameters. Beven and Binley (1992) noted that many models are over-parameterized and have drawn attention to the issue of equifinality: various combinations of model parameter values may yield similar results. Remote sensing data may be used to provide (initial) values of model parameters (NDVI, LAI, f_c) and may be used to correct state variables in the model.

Nocturnal transpiration. Night-time transpiration has been widely observed using sap-flow and gas exchange measurements, with ratios of night-time to day-time transpiration as large as 25% being reported (Dawson et al. 2007). Summer values of this ratio are more typically in the range of 10–20%, decreasing to less than 5% in winter. Such ratios have been reported for a wide variety of ecosystems (see Dawson et al. 2007). Nocturnal transpiration is correlated with increases in nocturnal vapour pressure deficit (i.e. $e_a^* - e_a$) and u, explaining respectively 54% and 37% of the observed variation from a well-watered site in south-east Australia (Benyon 1999). If nocturnal transpiration occurs at sites with high LAI (meaning daytime soil E is likely to be low) then this process, which is *not* usually modeled, could be an important source of error in remote sensing based estimates of E_a. Conversely, at sites with low LAI, likely increases in daytime soil E will tend to reduce this source of error so that it may be ignored when considering daily TIR-based estimates of E_a.

Diffuse radiation. On cloudy days diffuse light usually dominates, whereas direct light is dominant on clear days when most TIR data are acquired for use in modelling applications. In most SEB models only the total R_n flux is considered, and not the relative fractions of diffuse and direct radiation. Most SEB models use daytime data obtained for clear-sky conditions and the fact that the direct component is greater than the diffuse component has little impact. However, if one wants to develop a system to continuously monitor the water balance, the consequences of an increased diffuse fraction need to be considered, because the vegetation uses diffuse radiation more efficiently than direct

radiation (see Roderick et al. 2001 and the references therein). To ignore such differences in water use efficiency would lead to significant differences in estimates of E.

Most SEB models have been developed for use in cloud-free conditions and do not differentiate between direct and diffuse radiation, with one recent exception. At a rangeland site Anderson et al. (2008) incorporated an analytical light use efficiency (LUE) model developed by Anderson et al. (2000) into ALEXI and found that the error in 30-min flux estimates was reduced from 16% to 12%. Current research (Anderson, pers. comm. 2008) focuses on implementing and assessing the use of the LUE approach at the continental scale to account for differences in light use efficiency when the record of remotely sensed observations has gaps associated with cloud.

Dew. Early-morning dew on the vegetation surface has received little attention when using satellite based T_{rad} data for estimating E. Using ground based spectral radiometers, Pinter (1986) showed that there was no measurable change in radiant temperature of well-watered wheat transpiring at near-potential rates with and without dew. However, if the vegetation were not well-watered, then it is expected that the presence of dew would impact the satellite measurement of T_{rad} and ultimately E. This potential impact would be greater for satellite data acquired mid-morning (e.g. Landsat) compared to those commonly acquired mid-afternoon (e.g. AVHRR). Given the wide variety of methods to estimate E fusing data from different parts of the electromagnetic spectrum, the impact of dew on early-morning passive microwave (e.g., Wigneron et al. 1996) and reflective (e.g., Pinter 1986; Heusinkveld et al. 2008) data also needs to be acknowledged.

Limitations of satellite coverage. Satellites providing high spatial resolution imagery usually have lower temporal frequency; conversely low spatial resolution is usually associated with increased frequency. Different applications need different spatial and temporal coverage rates and require different "turn-around" times. If acquiring the imagery and applying the E estimation method requires too much time, the method becomes less attractive for operational applications as for example in determining water requirements in irrigated agriculture.

Another important issue for optical remote sensing is that the presence of clouds results in intermittent coverage so that many data applications and model validations are biased towards clear sky conditions. Intermittent coverage makes application of TIR methods in tropical regions such as Papua New Guinea quite unreliable and impractical; though environmental metrics such as T_{rad}/NDVI derived from monthly and longer composite AVHRR imagery have provided regional-level information about drought in such cloudy regions (McVicar and Bierwirth 2001). It also highlights the need for: (i) gap filling procedures such as described by Anderson (2007a, b); and (ii) coupling models based on TIR remote sensing with data obtained with passive microwave sensors which have lower spatial resolution but are not affected by cloud (Renzullo et al. 2008).

Finally, few studies report on the use of data from different satellite/sensor systems although there are significant differences in wavelength and resolution between various satellite/sensor systems which point to opportunities for data fusion (see Courault et al. 2005; Kustas et al. 2003c; McCabe et al. 2008b).

9.2 Evaluation of Remote Sensing Based Approaches

To date, there exist no effective means of evaluating spatially distributed outputs of either remote sensing based approaches or LSMs at scales greater than a few kilometers—particularly over non-homogeneous surfaces.

In order to assess their performance, remote sensing approaches and LSMs are routinely evaluated against each other (see for example French et al. 2005; Olioso et al. 2002b) or against ground based localized flux measurements with eddy covariance techniques (see for example Twine et al. 2000), Bowen ratio approaches and scintillometry (de Bruin et al. 1996; Green et al. 2001) or lysimeter techniques. It may be noted here that the uncertainty associated with Bowen ratio and eddy covariance measurements has been given at about 20% (see Kustas and Norman 1996; Norman et al. 1995, Farahani et al. 2007; Twine et al. 2000).

Glenn et al. (2007) described recent developments in the use of flux towers equipped with Bowen ratio or eddy covariance instrumentation. They noted that the number of flux tower installations is increasing every year and reported that data sets comprising several years of energy, water vapor and CO_2 flux measurements are now available for some 250 locations worldwide.

Even with these well developed and well established approaches, the accuracy of assessments is generally only within 10% (see Glenn et al. 2007), which is likely to diminish dramatically as the complexity of a landscape increases and/or meteorological conditions change away from the tower. The accuracy is also completely reliant on an effective and regular calibration procedure—which is very variable for some of the AmeriFlux or FluxNet data. This point was illustrated by Wilson et al. (2002) who reported an imbalance of 20% across 22 FLUXNET eddy correlation sites due to non-closure of the energy balance.

There are also few studies which address the representativeness of tower sites, especially in complex terrain. An example of one such study is Pypker et al. (2007) who used 10 and 28 m towers to observe the importance of cold air drainage in a steeply sided forested watershed.

It must be noted here that evaluation of remote sensing based approaches with ground based data tends to favor those few clear sky days when fluxes are reproduced most agreeably, and relatively flat locations where flux towers are overwhelmingly located. As a result, routine estimation of E using T_{rad} is constrained to some extent by issues of measurement scale i.e. the length scale of the underlying land surface unit that can be accurately monitored using ground based techniques and the time scale controlled by cloudiness conditions and satellite repeat characteristics.

In Table 2 the results of about 30 validation studies are summarized in which remote sensing based estimates are compared with ground based measurements of evaporation. These measurements have been made with eddy covariance and/or Bowen ratio equipment on masts or flux towers. Each entry provides references to the original study with a description of the technique and to the paper with the actual validation as well as details on land surface type, the source of the sources of the necessary data and the time step. For each validation the Table lists, where available, RMSE, r^2 value and the relative error.[7] Table 2 indicates that agreement between estimates and observations is reasonable with r^2 values in the 0.65–0.96 range. It shows that most techniques have uncertainties in the 15–30% range which is in broad agreement with Verstraeten et al. (2008), Glenn et al. (2007) and Jiang et al. (2004) who report uncertainties of 20–30%.The one paper describing assimilation of land surface temperatures in a land surface energy balance model (Caparrini et al. 2004) shows validation results which are comparable with other remote sensing techniques.

[7] RMSE = Root Mean Square Error = square root of the mean of the squares of the differences between estimate and observation; r = correlation coefficient and r^2 = coefficient of determination; and Relative Error = estimation error = (RMSE/mean value) $\times$100%.

Table 2 Validation of remote sensing techniques for estimating evaporation

Section	Method	Source	Validation	Surface type	T_{rad}, NDVI and albedo	$R_n - G$	E	Time step	RMSE (W m^{-2})	r^2	Relative error (%)
4.1	One-source SEB	Kustas (1990)	Kustas (1990)	Furrowed cotton	Mast; aircraft	Observed	BR EC	30 min	24–85		10–25
4.1	One-source SEB	Boegh et al. (2002)	Boegh et al. (2002)	Wheat, grass, maize, barley	Landsat TM	Derived	EC	30 min	27	0.87	14
4.1	One-source SEB	Su (2002)	Su et al. (2005)	Corn	Mast	Observed	EC	30 min	47	0.89	
4.1	One-source SEB	Su (2002)	Su et al. (2005)	Soybean	Mast	Observed	EC	30 min	40	0.84	
4.1	One-source SEB	Su (2002)	McCabe and Wood (2006)	Corn and soybean	ASTER	Derived	EC	Instant	99	0.66	
4.1	One-source SEB	Su (2002)	McCabe and Wood (2006)	Corn and soybean	Landsat 7 ETM	Derived	EC	Instant	68	0.77	
4.1	One-source SEB	Su (2002) [SEBS]	Su et al. (2007)	Grassland, crops, (rain)forest	MODIS	Derived	EC	Daily	44		25
4.2	Two-source SEB	Kustas (1990)	Kustas (1990)	Furrowed cotton	Mast, aircraft	Observed	BR EC	30 min	48		15
4.2	Two-source SEB	Norman et al. (1995) [TSM]	Kustas and Norman (1999)	Furrowed cotton	Masts; aircraft	Observed	BR EC	Instant	37–47		12–15
4.2	Two-source SEB	Norman et al. (1995) [TSM]	Norman et al. (2000)	Shrubland, rangeland, pasture, salt cedar	Masts	Derived	BR EC	30 min	105		27
4.2	Two-source SEB	Norman et al. (1995) [TSM]	French et al. (2005)	Corn and soybean	ASTER	Derived	EC	30 min	94		26
4.2	Two-source SEB	Kustas and Norman (1999)	Li et al. (2006)	Corn and soybean	Landsat7 ETM, Landsat5TM	Observed	EC	30 min	50–55		10–15
5	Time-rate of change	Anderson et al. (1997) [ALEXI], Norman et al. (2003)[disALEXI]	Norman et al. (2003)	Wheat, pasture	GOES, Airborne TIMS, TMS	Derived	EC	Hourly	40–50		20

Table 2 continued

Section	Method	Source	Validation	Surface type	T_{rad}, NDVI and albedo	$R_n - G$	E	Time step	RMSE (W m^{-2})	r^2	Relative error (%)
5	Time-rate of change	Norman et al. (2000) [DTD]	Norman et al. (2000)	Shrubland, rangeland, pasture, bare, salt cedar	IRT on masts	Derived	BR EC	30 min	65		17
5	Time-rate of change	Anderson et al. (1997) [ALEXI], Norman et al. (2003)[disALEXI]	Anderson et al. (2007a, b)	Water, forest, woodland, shrubland, grassland, crops, bare, built-up	GOES, MODIS	Derived	EC	Hourly	58		25
6.1	T_{rad}, α and VIs	Bastiaanssen et al. (1998a) Bastiaanssen (2000) [SEBAL]	French et al. (2005)	Corn and soybean	ASTER	Derived	EC	30 min, during overpass	55		15
6.2	T_{rad} and α	Roerink et al. (2000) [S-SEBI]	Verstraeten et al. (2005)	Forests	AVHRR	Derived	EC	30 min during overpass	35		24
6.3	T_{rad} and VIs	Carlson et al. (1995a) [Triangle Method]	Gillies et al. (1997)	Tallgrass prairie, grasslands, steppeshrub	Aircraft M/S scanner	Observed	BR EC	During overpass	25–55	0.80–0.90	10–30
6.3	T_{rad} and VIs	Jiang and Islam (2001)	Jiang and Islam (2001)	Mixed farming, forest, tall & short grass	AVHRR	Derived	BR EC	During overpass	85	0.64	30
6.3	T_{rad} and VIs	Jiang and Islam (2001)	Jiang and Islam (2001)	Mixed farming, forest, tall &short grass	AVHRR	Observed	BR EC	During overpass	50	0.90	17
6.3	T_{rad} and VIs	Jiang and Islam (2001)	Jiang and Islam (2003)	Mixed farming, cropping, forest, tall& short grass	AVHRR	Derived	BR EC	During overpass	59	0.79	15

Table 2 continued

Section	Method	Source	Validation	Surface type	T_{rad}, NDVI and albedo	$R_n - G$	E	Time step	RMSE (W m^{-2})	r^2	Relative error (%)
6.3	T_{rad} and VIs	Jiang and Islam (2001)	Batra et al. (2006)	Mixed farming, forest, tall &short grass	MODIS, AVHRR	Derived	BR	During overpass	51–56	0.77–0.84	22–28
6.3	T_{rad} and VIs	Nishida et al. (2003a)	Nishida et al. (2003a)	Forest, corn, soybean, wheat, shrubland rangeland, tallgrass	AVHRR	Derived	EC	Day time averages	45	0.86	
6.4	Empirical method based on EVI	Wang et al. (2007)	Wang et al. (2007)	Forest, grassland, cropping	MODIS	Observed	EC	16-day averages	32	0.81	36
7.2	T_{rad} and climate data	McVicar and Jupp (2002) [NDTI]	McVicar and Jupp (1999)	Cropping	Mast IRT	Observed	BR	AVHRR and TM overpass time	88–72	0.52–0.81	27–30
7.3	T_{rad} and compl. approach	Granger (1989) [Complementary method]	Crago and Crowley (2005)	Grassland, rangelands	Mast IRT	Observed	EC BR	10 min, 30 min	16–132		
7.3	T_{rad} and compl. approach	Venturini et al. (2008)	Venturini et al. (2008)	Rangelands, pasture, wheat	MODIS	Derived	BR	Instant. on 7 days	34	0.79	15
8.2	Assimilation of T_{rad}	Caparrini et al. (2004)	Caparrini et al. (2004)	Tall-grass prairie	IRT on masts	Observed	EC BR	30 min	56		
8.2	Assimilation of T_{rad}	Caparrini et al. (2004)	Caparrini et al. (2004)	Tall-grass prairie	IRT on masts	Observed	EC BR	Daily averages	20	0.96	

The uncertainties shown here will depend on whether the available energy ($R_n - G$) used in estimating evaporation is derived from satellite data (see Sect. 2) or obtained from ground based measurements. For example, Jiang and Islam (2001) reported that use of ground based ($R_n - G$) observations rather than values derived from remote sensing did improve the accuracy of the remote sensing technique as shown by the decrease in the relative error from 30% down to 17%. It should also be noted that the ($R_n - G$) term used in the Bowen Ratio or eddy covariance approaches to measuring evaporation is always based on ground based observations.

These validations indicate that there is a need to develop an effective framework to validate land surface models beyond the standard field scale because modelling approaches are usually employed at regional scales.

This review has also shown that the distributed nature of remote sensing observations has not yet been utilized effectively to evaluate and improve land surface model simulations, though early promising approaches have been developed. The inability to evaluate remote sensing based estimates in a distributed manner is a serious limitation in broader scale applications of such approaches.

Estimates of evaporation (E) may be evaluated from rainfall (P) and streamflow (Q) over longer periods by closing the water balance expressed by $E = P - Q - dS/dt$, provided the spatial and temporal variability of rainfall is known and temporal changes in the soil moisture store (dS/dt) can be ignored by assuming steady state conditions. However, at shorter time scales, dS/dt becomes increasingly important (e.g. Brown et al. 2005; McVicar et al. 2007c) and must be accounted for. It is also noted that there would be serious difficulties with such evaluation in regions with significant and/or variable groundwater exploitation. Another fully independent validation approach at monthly time scales for very large river basins could be if dS/dt is estimated through deconvolution of the gravity field from GRACE accelerometer measurements (see for example Rodell et al. 2004).

Finally, there have also been some efforts to explore more semi-qualitative based approaches. The concept of hydrological consistency (McCabe et al. 2008b) is one that has recently been introduced to provide a means of evaluating/validating LSMs. The search for hydrological consistency is fundamentally an effort to seek improvement in hydrological simulation, through ensuring concurrence between independent observations of water and energy cycle variables rather than reliance solely on single-process and single-variable oriented approaches.

9.3 Temporal and Spatial Scaling Issues

All the methods described in Sects. 4–7 provide instantaneous E estimates at the time of satellite overpass whereas most applications in irrigated agriculture and in hydrology require E values over daily or longer time periods. This requires extrapolation from instantaneous values to daily time steps, and beyond. Such temporal scaling has been implemented with analytical expressions based on the assumption that the temporal trend in λE throughout the day follows the course of $K\downarrow$ (see Jackson et al. 1983) or of R_n (see Seguin and Itier 1983; Sanchez et al. 2008).

An alternative, and more widely used, approach to temporal scaling is based on the observation (see for example Crago 1996; Crago and Brutsaert 1996; Caparrini et al. 2004) that for unstressed vegetation the evaporative fraction Λ remains fairly constant for most of the day-light hours, and especially from mid-morning to mid-afternoon. Λ may thus be calculated when R_n, G and H are estimated at the time of satellite overpass. Hence, with a known Λ value, the instantaneous E value can be scaled up to daily values if the R_n is

known over 24 h, with the assumption that G is negligible over the diurnal cycle or by considering the phase difference between R_n and G (Gentine et al. 2007). The accuracy of the constant evaporative fraction approach has been estimated to be better than ±1 mm/day (Hall et al. 1992; Kustas et al. 1994b).

Another approach to temporal scaling is to hold the ratio between the actual E and some potential or reference E, i.e. $E_a/E_{ref,}$ constant between successive remote sensing observations and to update the ratio when a new estimate of E_a is available with new remote sensing observations. For example in SEBAL the surface resistance r_s is kept constant between remote sensing observations so that the Penman–Monteith expression can be used to estimate E_p and E_a between successive remote sensing observations. METRIC (see Allen et al. 2007a) uses a reference crop E to extrapolate instantaneous E_a estimates to daily rates.

Most E models are assumed to be scalable in geographic space; that is, it is assumed that they can operate across field scales and larger. That surface temperature scales non-linearly and cannot simply be upscaled (e.g. McCabe et al. 2008a), as is the case with many other forcing variables and parameters (Garratt and Prata 1996; Moran et al. 1997), makes this assumption difficult to verify. Many methods, or models, that work well at the local scale may become unreliable when used at regional and larger scales and over non-homogeneous land surfaces. This may be caused by poor model initialization, unrepresentative values for the key model parameters, or more generally, a lack of knowledge of the dominant physical processes operating at different scales. Further, whether models are capable of multi-scale estimates is difficult to verify, given that evaluation of models generally only ever takes place at the field scale and for intensive field campaigns (e.g. Norman et al. 2003; Kustas et al. 2004; Su et al. 2005; Verstraeten et al. 2008).

The possibility of resolving these questions is complicated by the lack of an appropriate scaling theory in hydrology (Beven and Fisher 1996) which limits the effective synthesis of multi-resolution data. Generally, spatial scaling studies have focused on a single sensor, progressively degrading the pixel size to mimic expected results from sensors with coarser resolution (Kustas et al., 2004; Li et al. 2005; 2008). Some recent efforts have attempted to address scaling by analyzing remotely based estimates of E from independent multi-resolution satellite sensors. McCabe and Wood (2006) employed data from Landsat-ETM, ASTER and MODIS to independently estimate land surface fluxes, allowing direct comparison of results across measurement resolutions. Like Kustas et al. (2004) and Li et al. (2008) who used aggregated Landsat data, McCabe and Wood found that while high resolution data accurately reproduced tower based retrievals, the coarser scale data showed less agreement. However, they also found that the catchment average evaporation was well maintained with all three satellite platforms, indicating the potential utility of MODIS scale retrievals for water management applications.

Figure 6 details maps of λE derived from McCabe and Wood (2006), illustrating the consistency in the high resolution retrievals, and also the removal of high resolution structure from the coarser scale MODIS retrievals.

At the other end of the scale it has also been observed that large scale methods such as ALEXI, need to be disaggregated (see disALEXI) before their output can be used and/or validated at the regional or local scale (see Norman et al. 2003; Kustas et al. 2003c). There is a need for approaches that utilize low-resolution (greater than 1 km) satellite platforms, to inform upon the field scale. Indeed, the use of high-temporal/low-spatial resolution geostationary platforms has been limited in land surface hydrological studies. Approaches that merge the interests of larger scale hydrological and climatological research, with the needs of irrigation and water resource managers, offer an excellent means to address the competing needs of these communities.

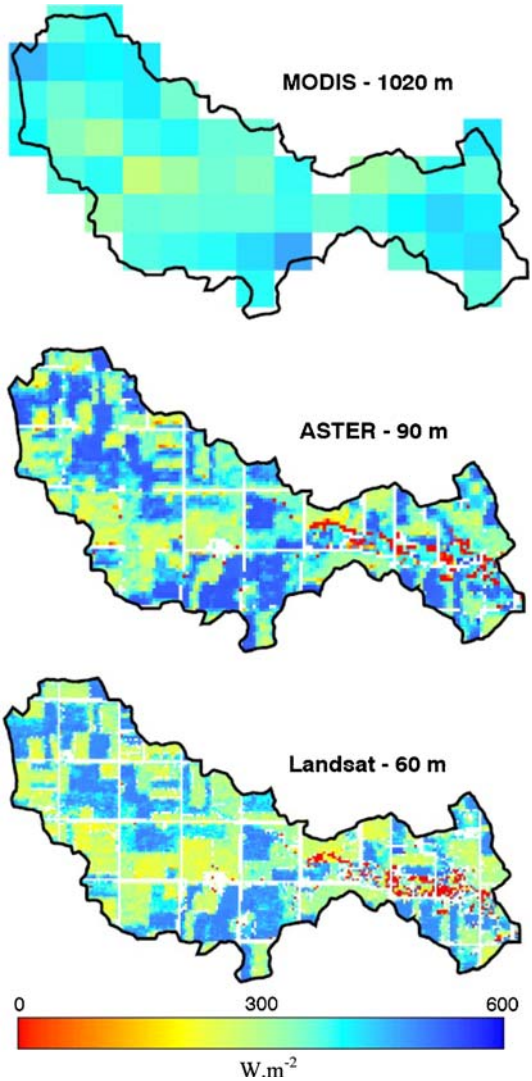

Fig. 6 The influence of scale on E estimates using Landsat, ASTER and MODIS based retrievals (Fig. 3 from McCabe and Wood 2006). Instantaneous retrievals from 1 July 2002 are presented for a small (14 km^2) watershed within the SMACEX-02 field experiment (Kustas et al. 2005) at 60 m, 90 m and 1020 m resolution. As in Fig. 3c, results illustrate good agreement and consistency at high resolutions, but less so at coarser scales (>1 km). These coarse scale measurements however, were shown to provide good characterization of the catchment average E, highlighting the utility of remote sensing approaches in water resource management and related hydrological applications

It must also be noted in the context of data fusion that joint use of data from different sensors makes it necessary to consider discrepancies in land surface temperatures. For example Liu et al. (2007) recently compared several correction approaches to reduce discrepancies in T_{rad} observed with MODIS and ASTER which have complementary resolutions of 960 m and 90 m, respectively.

10 Concluding Remarks

From this review a brief listing of residual challenges and future directions follows:

(i) remote sensing approaches for estimating E are used in several areas including (a) irrigation management and crop water demand assessment, (b) plant growth, carbon and

nutrient cycling and production modelling in dry land agriculture and forestry, (c) catchment hydrology, and (d) larger scale meteorology and climatology applications;
(ii) areal E values are needed in each application area. Remote sensing can make a major contribution towards understanding the spatial variability in land surface fluxes and in arriving at representative areal values;
(iii) in the context of irrigated agriculture, evaporation data is used at high spatial and temporal resolutions and the utility of remote sensing approaches is therefore largely controlled by the satellite's return rate and cloud conditions. For most practical purposes the twice-monthly (at best) temporal response of high-resolution platforms (ASTER and Landsat) is inadequate, so these approaches rely upon the development of improved methods for temporal extrapolation to achieve at least daily values;
(iv) while lacking high resolution spatial detail, for applications in catchment hydrology as well as meteorological and climatological applications, daily 1 km resolution MODIS and/or AVHRR data can provide good estimates of the catchment's average evaporation on a daily basis subject to cloud cover, thus providing a valuable data source, particularly for flood forecasting, drought detection, weather prediction, and other land and water management issues. Geostationary platforms offer increasingly improved spatial resolutions ($\sim$5 km) with unsurpassed temporal frequency (up to 15 min), but remain an under-utilized resource;
(v) for larger scale applications in meteorology and climatology "operational" evaporation models are required which couple land surface and atmospheric models and may be used at a range of spatial (regional, continental, global) and temporal (days, weeks, months) scales. Such models require routine data input at daily time steps and will increasingly use data from geostationary satellites in order to avoid being constrained by once-daily overpasses.
(vi) there are considerable errors associated with using surface temperatures to estimate sensible heat flux because of significant inaccuracies in T_{rad} observations, the inequality between T_{rad} and T_{aero}, and the temporal and spatial variability in the difference between T_{rad} and T_{aero}. There are also errors in estimating the available energy ($R_n - G$) and other ground based meteorological observations, as well as errors due to various model assumptions. This paper reports on several approaches which are aimed at reducing the impact of those uncertainties;
(vii) Seguin et al. (1999) found that the majority of published remote sensing methods for estimating E had an accuracy of $\pm$80–90 W m^{-2} or 1.5 mm day^{-1}. They noted that more precise evaluation was needed at various scales and suggested that E flux retrieval accuracy for many agricultural and hydrological applications should have an accuracy of $\sim$50 W m^{-2} or 0.8 mm day^{-1} at the field scale, although this will vary with individual applications;
(viii) the present paper lists some 30 validations of remote sensing approaches for estimating E which report on average an RMSE of just over 50 W m^{-2}. A surprising feature is that the more complex physical and analytical methods are not necessarily more accurate than statistical or empirical methods, such as the methods described in Sect. 6.5. However, the datasets required to force (or train) some of the empirical methods are not available everywhere;
(ix) comparisons with ground based measurements which themselves have a reported uncertainty of 10–15%, indicate that the various remote sensing techniques for estimating E have uncertainties of 15–30%;
(x) intermittent satellite coverage due to the presence of clouds results in E estimation which is biased to clear and dry days. Intermittent coverage emphasizes the need to

develop gap filling procedures. There is also a need for considering the relative fractions of direct and diffuse radiation which are dependent on cloud cover and their impact on water use by vegetation. Evaluation over cloudy and non-cloudy periods will likely adjust the reported accuracies of the various remote sensing approaches;
(xi) there is a need for improved temporal scaling procedures to extrapolate instantaneous estimates of evaporation obtained at the time of the satellite overpass to E values for hourly, daily or longer time periods. Temporal scaling also needs to consider the importance of nocturnal transpiration;
(xii) extrapolation of daily values to weekly totals and beyond must be based on integrated E values rather than the use of averaged surface temperature values which are strongly biased towards days with minimal cloud cover;
(xiii) remote sensing can provide area-average values of surface fluxes at the relevant scale. However, aggregation rules are needed for (a) uniform terrain and land cover, (b) over mixed vegetation with length scales of less than 10 km, and (c) for land cover which is organized at a scale of at least 10 km (see Shuttleworth 1991);
(xiv) large-area applications of the methods described in Sects. 3–8 are hampered by the lack of appropriate ground based observations (e.g. air temperature, wind speed and solar radiation at the time of T_{rad} data acquisition) although methods are available to estimate these from daily extreme and integral ground based observations and by limited information on land surface characteristics (e.g. surface roughness length and vegetation properties);
(xv) only a small number of studies have reported on the use of data from satellite/sensor systems with significant differences in wavelength and resolution which point to opportunities for data fusion. Such data fusion would allow for representative areal values to be derived as well as the links between large scale and regional-scale E estimation and other components of the hydrological cycle to be investigated; and
(xvi) data fusion approaches may assist in the synthesis of multi-resolution data, in the development of a theory of scale dependence and in testing hypotheses for obtaining representative areal values of evaporation for homogeneous and heterogeneous landscapes and vegetation cover.

While we acknowledge that the collective journey of using thermal remote sensing to estimate regional (and larger scale) evaporation will undoubtedly pose more research questions than listed here, we also note the current increased utility of thermal remote sensing based E estimates in operational monitoring and decision support systems, illustrating the significant advances that have been made in three decades of research and investigation.

Acknowledgements The authors wish to thank Wim Bastiaanssen, Gilles Boulet, Huub Savenije and two anonymous referees for their useful comments on earlier drafts of this paper.

References

Allen RG, Pereira LS, Raes D, Smith M (1998) Crop evapotranspiration—guidelines for computing crop water requirements. FAO irrigation and drainage paper 56, Rome, Italy http://www.fao.org/docrep/X0490E/X0490E00.htm

Allen RG, Tasumi M, Trezza R (2007a) Satellite-based energy balance for mapping evapotranspiration with internalized calibration (METRIC): model. J Irrig Drain Eng 133(4):380–394. doi:10.1061/(ASCE)0733-9437(2007)133(4):(380)

Allen RG, Tasumi M, Trezza R (2007b) Satellite-based energy balance for mapping evapotranspiration with internalized calibration (METRIC): applications. ASCE J Irrig Drain Eng 133(4):395–406

Anderson MC, Norman JM, Diak GR, Kustas WP, Mecikalski JR (1997) A two-source time-integrated model for estimating surface fluxes from thermal infrared satellite observations. Remote Sens Environ 60:195–216. doi:10.1016/S0034-4257(96)00215-5

Anderson MC, Norman JM, Meyers TP, Diak GR (2000) An analytical model for estimating canopy transpiration and carbon assimilation fluxes based on canopy light-use efficiency. Agric For Meteorol 101:265–289. doi:10.1016/S0168-1923(99)00170-7

Anderson MC, Norman JM, Mecikalski JR, Otkin JA, Kustas WP (2007a) A climatological study of evapotranspiration and moisture stress across the continental United States based on thermal remote sensing: 1 Model formulation. J Geophys Res 112:D10117. doi:10.1029/2006JD007506

Anderson MC, Norman JM, Mecikalski JR, Otkin JA, Kustas WP (2007b) A climatological study of evapotranspiration and moisture stress across the continental United States based on thermal remote sensing: 2 Surface moisture climatology. J Geophys Res 112:D10117. doi:10.1029/2006JD007507

Anderson MC, Kustas WP, Norman JM (2007c) Upscaling flux observations from local to continental scales using thermal remote sensing. Agron J 99:240–254

Anderson MC, Norman JM, Kustas WP, Houborg R, Starks PJ, Agam N (2008) Mapping coupled carbon and water fluxes at the land surface using thermal and optical remote sensing data. Remote Sens Environ (in press)

Bastiaanssen WGM (2000) SEBAL-based sensible and latent heat fluxes in the irrigated Gediz Basin, Turkey. J Hydrol (Amst) 229:87–100. doi:10.1016/S0022-1694(99)00202-4

Bastiaanssen WG, Hoekman DH, Roebeling RA (1994) A methodology for the assessment of surface resistance and soil water storage variability at mesoscale based on remote sensing measurements. IAHS Special Publication No. 2, IAHS Press, Institute of Hydrology, Wallingford

Bastiaanssen WGM, Menenti M, Feddes RA, Holtslag AAM (1998a) A remote sensing surface energy balance algorithm for land. I. Formulation. J Hydrol (Amst) 212/213:198–212. doi:10.1016/S0022-1694(98)00253-4

Bastiaanssen WGM, Pelgrum H, Wang J, Ma Y, Moreno JF, Roerink GJ (1998b) A remote sensing surface energy balance algorithm for land (SEBAL) 2 Validation. J Hydrol (Amst) 212/213:213–229. doi:10.1016/S0022-1694(98)00254-6

Batra N, Islam S, Venturini V, Bisht G, Jiang L (2006) Estimation and comparison of evapotranspiration from MODIS and AVHRR sensors for clear sky days over the Southern Great Plains. Remote Sens Environ 103:1–15. doi:10.1016/j.rse.2006.02.019

Benyon RG (1999) Nighttime water use in an irrigated Eucalyptus grandis plantation. Tree Physiol 19:853–859

Beven KJ, Binley AM (1992) The future of distributed models: model calibration and uncertainty prediction. Hudrological processes 6:279–298

Beven KJ, Fisher J (1996) Remote sensing and scaling in hydrology. In: Stewart JB, Engman ET, Feddes RA, Kerr Y (eds) Scaling up in hydrology using remote sensing. Wiley, Chichester, UK

Bhumralkar CM (1975) Numerical experiments on the computation of ground surface temperature in an atmospheric general circulation model. J Appl Meteorol 14:1246–1258. doi :10.1175/1520-0450(1975)014<1246:NEOTCO>2.0.CO;2

Bisht G, Venturini V, Islam S, Jiang L (2005) Estimation of the net radiation using MODIS (Moderate Resolution Imaging Spectroradiometer) data for clear sky days. Remote Sens Environ 97:52–67. doi:10.1016/j.rse.2005.03.014

Boegh E, Soegaard H, Hanan N, Kabat P, Lesch L (1999) A remote sensing study of the NDVI–T_s relationship and the transpiration from sparse vegetation in the Sahel based on high-resolution satellite data. Remote Sens Environ 69:224–240. doi:10.1016/S0034-4257(99)00025-5

Boegh E, Soegaard H, Thomsen A (2002) Evaluating evapotranspiration rates and surface conditions using Landsat TM to estimate atmospheric resistance and surface resistance. Remote Sens Environ 79:329–343. doi:10.1016/S0034-4257(01)00283-8

Bouchet RJ (1963) Evapotranspiration réelle et potentielle, signification climatique. International Association of Hydrological Sciences, Proceedings of General Assembly, Berkeley, California Symposium. Publication 62:134–142

Boulet G, Kalma JD, Braud I, Vauclin M (1999) Towards effective parameterization of soil physical and land surface properties in regional water balance studies. J Hydrol (Amst) 217:225–238. doi:10.1016/S0022-1694(98)00246-7

Boulet G, Chehbouni A, Gentine P, Duchemin B, Ezzahar J, Hadria R (2007) Monitoring water stress using time series of observed to unstressed surface temperature difference. Agric For Meteorol 146(3–4):159–172

Braden H, Blanke T (1993) About the use of remotely sensed surface temperatures for controlling estimates of evapotranspiration. Model Geo-Biosphere Process Ger 2:53–66

Brotzge JA, Richardson S, Crawford K, Horst T, Brock F, Humes K (1999) The Oklahoma Atmospheric Surface-Layer Instrumentation System (OASIS) project. In: Proceedings of 13th symposium on boundary layers and turbulence, Dallas, TX, 10–15 January 1999. American Meteorological Society, Boston, MA, pp 612–615

Brown AE, Zhang L, McMahon TA, Western AW, Vertessy RA (2005) A review of paired catchment studies for determining changes in water yield resulting from alterations in vegetation. J Hydrol (Amst) 310:28–61. doi:10.1016/j.jhydrol.2004.12.010

Brutsaert W (1982) Evaporation into the atmosphere. D. Reidel Publishing Company, Dordrecht, Holland, 299 pp

Brutsaert W (1999) Aspects of bulk atmospheric boundary layer similarity under free-convective conditions. Rev Geophys 37:439–451. doi:10.1029/1999RG900013

Caparrini F, Castelli F, Entekhabi D (2003) Mapping of land-atmosphere heat fluxes and surface parameters with remote sensing data. Boundary-Layer Meteorol 107:605–633. doi:10.1023/A:1022821718791

Caparrini F, Castelli F, Entekhabi D (2004) Estimation of surface turbulent fluxes through assimilation of radiometric surface temperature sequences. J Hydrometeorol 5:145–159. doi :10.1175/1525-7541(2004)005<0145:EOSTFT>2.0.CO;2

Carlson TN (1986) Regional scale estimation of surface moisture availability and thermal inertia using remote thermal measurements. Remote Sens Rev 1:197–247

Carlson TN (2007) An overview of the "triangle method" for estimating surface evapotranspiration and soil moisture from satellite imagery. Sensors 7:1612–1629

Carlson TN, Capehart WJ, Gillies RR (1995a) A new look at the simplified method for remote sensing of daily evapotranspiration. Remote Sens Environ 54:161–167. doi:10.1016/0034-4257(95)00139-R

Carlson TN, Gillies RR, Schmugge TJ (1995b) An interpretation of methodologies for indirect measurement of soil water content. Agric For Meteorol 77:191–205. doi:10.1016/0168-1923(95)02261-U

Castellví F, Stockle CO, Perez PJ, Ibañez M (2001) Comparison of methods for applying the Priestley–Taylor equation at a regional scale. Hydrol Process 15:1609–1620. doi:10.1002/hyp. 227

Choudhury BJ (1983) Simulating the effects of weather variables and soil water potential on a corn crop canopy temperature. Agric Meteorol 29:169–182. doi:10.1016/0002-1571(83)90064-X

Choudhury BJ (1989) Estimating evaporation and carbon assimilation using infrared temperature data Vistas in Modeling. In: Asrar G (ed) Theory and applications of optical remote sensing. Wiley, New York, pp 628–690

Choudhury BJ, De Bruin HAR (1995) First-order approach for estimating unstressed transpiration from meteorological satellite data. Adv Space Res 16(10):167–176. doi:10.1016/0273-1177(95)00398-X

Cleugh HA, Leuning R, Mu Q, Running SW (2007) Regional evaporation estimates from flux tower and MODIS satellite data. Remote Sens Environ 106:285–304. doi:10.1016/j.rse.2006.07.007

Coll C, Caselles V, Galve JM, Valor E, Niclos R, Sanchez JM (2005) Ground measurements for the validation of land surface temperatures derived from AATSR and MODIS data. Remote Sens Environ 97:288–300. doi:10.1016/j.rse.2005.05.007

Courault D, Seguin B, Olioso A (2005) Review on estimation of evapotranspiration from remote sensing data: from empirical to numerical modelling approaches. Irrig Drain Syst 19:223–249. doi:10.1007/s10795-005-5186-0

Crago RD (1996) Conservation and variability of the evaporative fraction during the daytime. J Hydrol (Amst) 180:173–194. doi:10.1016/0022-1694(95)02903-6

Crago RD, Brutsaert W (1996) Conservation and variability of the evaporative fraction during the daytime. J Hydrol 180:173–194

Crago RD, Crowley R (2005) Complementary relationships for near-instantaneous evaporation. J Hydrol (Amst) 300:199–211. doi:10.1016/j.jhydrol.2004.06.002

Crow WT, Wood EF, Pan M (2003) Multiobjective calibration of land surface model evapotranspiration predictions using streamflow observations and spaceborne surface radiometric temperature retrievals. J Geophys Res 108(23):4725. doi:10.1029/2002JD003292

Dash P, Gottschke F, Olesen F, Fischer H (2002) Land surface temperature and emissivity estimation from passive sensor data: theory and practice. Intern J. Rem. Sens 23:2563–2594. doi:10.1080/01431160110115041

Dawson TE, Burgess SSO, Tu KP, Oliveira RS, Santiago LS, Fisher JB (2007) Nighttime transpiration in woody plants from contrasting ecosystems. Tree Physiol 27:561–575

De Bruin HAR, Van den Hurk BJJM, Koshiek W (1996) The scintillation method tested over a dry vineyard area. Boundary-Layer Meteorol 76:25–40. doi:10.1007/BF00710889

Diak GR (1990) Evaluation of heat flux, moisture flux and aerodynamic roughness at the land surface from knowledge of the PBL height and satellite-derived skin temperatures. Agric For Meteorol 52:181–198. doi:10.1016/0168-1923(90)90105-F

Diak GR, Whipple MS (1993) Improvements to models and methods for evaluating the land surface energy balance and "effective" roughness using radiosonde reports and satellite-measured "skin" temperatures. Agric For Meteorol 63:189–218. doi:10.1016/0168-1923(93)90060-U

Farahani H, Howell T, Shuttleworth W, Bausch WC (2007) Evapotranspiration: progress in measurement and modeling in agriculture. Trans Am Soc Agric Biol Engineers 50:1627–1638

Flint AL, Childs SW (1991) Use of the Priestley–Taylor evaporation equation for soil water limited conditions in a small forest clearcut. Agric For Meteorol 56:247–260. doi:10.1016/0168-1923(91)90094-7

Franks SW, Beven KJ (1997) Bayesian estimation of uncertainty in land surface–atmosphere flux predictions. J Geophys Res 102(D20):23,991–23,999. doi:10.1029/97JD02011

Franks SW, Beven KJ (1999) Conditioning a multiple patch SVAT model using uncertain space–time estimates of surface fluxes as inferred from remotely sensed data. Water Resour Res 35(9):2751–2761. doi:10.1029/1999WR900108

French AN, Jacob F, Anderson MC, Kustas WP, Timmermans W, Gieske A (2005) Surface energy fluxes with the Advanced Spaceborne Thermal Emission and Reflection radiometer (ASTER) at the Iowa 2002 SMACEX site (USA). Remote Sens Environ 99(1–2):55–65. doi:10.1016/j.rse.2005.05.015

Friedl MA, Davis FW (1994) Sources of variation in radiative surface temperature over a tall grass prairie. Remote Sens Environ 48:1–17. doi:10.1016/0034-4257(94)90109-0

Garratt JR, Prata AJ (1996) Surface radiation budget: scaling up from local observations. In: Stewart JB, Engman ET, Feddes RA, Kerr Y (eds) Scaling up in hydrology using remote sensing. Wiley, pp 77–91

Gentine P, Entekhabi D, Chehbouni A, Boulet G, Duchemin B (2007) Analysis of evaporative fraction diurnal behaviour. Agric For Meteorol 143:13–29. doi:10.1016/j.agrformet.2006.11.002

Gillies RR, Carlson TN (1995) Thermal remote sensing of surface soil water content with partial vegetation cover for incorporation into climate models. J Appl Meteorol 34:745–756. doi :10.1175/1520-0450(1995)034<0745:TRSOSS>2.0.CO;2

Gillies RT, Carlson TN, Cui J, Kustas WP, Humes KS (1997) A verification of the "triangle" method for obtaining surface soil water content and energy fluxes from remote measurements of the Normalized Difference Vegetation Index (NDVI) and surface radiant temperatures. Int J Remote Sens 18(15):3145–3166. doi:10.1080/014311697217026

Glenn EP, Huete AR, Nagler PL, Hirschboeck KK, Brown P (2007) Integrating remote sensing and ground methods to estimate evapotranspiration. Crit Rev Plant Sci 26(3):139–168. doi:10.1080/07352680701402503

Gowda PH, Chavez JL, Colaizzi PD, Evett SR, Howell TA, Tolk JA (2007) Remote sensing based energy balance algorithms for mapping ET: current status and future challenges. Trans Am Soc Agric Biol Engineers 50(5):1639–1644

Granger RJ (1989) A complementary relationship approach for evaporation from non-saturated surfaces. J Hydrol (Amst) 111:31–38. doi:10.1016/0022-1694(89)90250-3

Green AE, Astill MS, McAneney KJ, Nieveen JP (2001) Path averaged surface fluxes determined from infrared and microwave scintillometers. Agric For Meteorol 109:233–247. doi:10.1016/S0168-1923(01)00262-3

Gupta HV, Sorooshian S, Yapo PO (1998) Toward improved calibration of hydrological models: multiple and non-commensurable measures of information. Water Resour Res 4:751–762. doi:10.1029/97WR03495

Haddeland I, Lettenmaier DP, Skaugena T (2006) Reconciling simulated moisture fluxes resulting from alternate hydrologic model time steps and energy budget closure assumptions. J Hydrometeorol 7(3):355–370. doi:10.1175/JHM496.1

Hall FG, Huemmrich RH, Goetz SJ, Sellers PJ, Nickerson JE (1992) Satellite remote sensing of surface energy balance: success, failures and unresolved issues in FIFE. J Geophys Res 97(D17):19,061–19,090

Heusinkveld BG, Berkowicz SM, Jacobs AFG, Hillen W, Holtslag AAM (2008) A new remote optical wetness sensor and its applications. Agric For Meteorol 148:580–591. doi:10.1016/j.agrformet.2007.11.007

Hobbins MT, Ramırez JA, Brown TC (2004) Trends in pan evaporation and actual evapotranspiration across the conterminous U.S.: paradoxical or complementary? Geophys Res Lett 31:L13503. doi:10.1029/2004GLO19846, 5 pp

Hook S, Prata AJ (2001) Land surface temperature measured by ASTER_First results. Geophysical research abstracts, 26th General Assembly, Vol. 3, p 71, European Geophysical Society

Hope AS, Petzold DE, Goward SN, Ragan RM (1986) Simulated relationships between spectral reflectance, thermal emissions, and evapotranspiration of a soybean canopy. Water Resour Bull 22:1011–1019
Houser PR, Shuttleworth WJ, Famiglietti JS, Gupta HV, Syed KH, Goodrich DC (1998) Integration of soil moisture remote sensing and hydrologic modeling using data assimilation. Water Resour Res 34(12):3405–3420. doi:10.1029/1998WR900001
Huang X, Lyons TJ, Smith RCG, Hacker JM, Schwerdtfeger P (1993) Estimation of the energy balance from radiant surface temperature and NOAA-AVHRR sensor reflectances over agricultural and native vegetation. J Appl Meteorol 32:1441–1449. doi :10.1175/1520-0450(1993)032<1441:EOSEBF>2.0.CO;2
Huete A, Didan K, Miura T, Rodrequez E, Gao X, Ferreira L (2002) Overview of the radiometric and biophysical performance of the MODIS vegetation indices. Remote Sens Environ 83:195–213. doi:10.1016/S0034-4257(02)00096-2
Jackson RD, Idso SB, Reginato RJ, Pinter PJ (1981) Canopy temperature as a crop water stress indicator. Water Resour Res 17:1133–1138. doi:10.1029/WR017i004p01133
Jackson RD, Hatfield JL, Reginato RJ, Idso SB, Pinter PJ (1983) Estimation of daily evapotranspiration from one time-of-day measurements. Agric Water Manage 7:351–362. doi:10.1016/0378-3774(83)90095-1
Jackson TJ, Le Vine DM, Hsu AY, Oldak A, Starks PJ, Swift CT (1999) Soil moisture mapping at regional scales using microwave radiometry: the Southern Great Plains hydrology experiment. IEEE Trans Geosci Rem Sens 37:2136–2151. doi:10.1109/36.789610
Jacob F, Petitcolin F, Schmugge T, Vermote E, Ogawa K, French A (2004) Comparison of land surface emissivity and radiometric temperature from MODIS and ASTER sensors. Remote Sens Environ 83:1–18
Jarvis PG, McNaughton KG (1986) Stomatal control of transpiration. Scaling up from leaf to region. Adv Ecol Res 15:1–49. doi:10.1016/S0065-2504(08)60119-1
Jiang L, Islam S (2001) Estimation of surface evaporation map over southern Great Plains using remote sensing data. Water Resour Res 37:329–340. doi:10.1029/2000WR900255
Jiang L, Islam S (2003) An intercomparison of regional latent heat flux estimation using remote sensing data. Int J Remote Sens 24(11):2221–2236. doi:10.1080/01431160210154821
Jiang L, Islam S, Carlson TR (2004) Uncertainties in latent heat flux measurement and estimation: implications for using a simplified approach with remote sensing data. Can J Rem Sens 30:769–787
Jones AS, Guch IC, VonderHaar TH (1998a) Data assimilation of satellite derived heating rates as proxy surface wetness data into a regional atmospheric mesoscale model. Part I: methodology. Mon Weather Rev 126:634–645. doi :10.1175/1520-0493(1998)126<0634:DAOSDH>2.0.CO;2
Jones AS, Guch IC, VonderHaar TH (1998b) Data assimilation of satellite derived heating rates as proxy surface wetness data into a regional atmospheric mesoscale model. Part II: case study. Mon Weather Rev 126:646–667. doi :10.1175/1520-0493(1998)126<0646:DAOSDH>2.0.CO;2
Jupp DLB, Kalma JD (1989) Distributing evapotranspiration in a catchment using airborne remote sensing. Asian-Pacific Remote Sens J 2:13–15
Jupp DLB, Tian G, McVicar TR, Qin Y, Fuqin L (1998) Soil moisture and drought monitoring using remote sensing I: theoretical background and methods. CSIRO Earth Observation Centre, Canberra http://www.eoc.csiro.au/pubrep/scirpt/jstc1.pdf
Kalma JD, Calder IR (1994) Land surface processes in large scale hydrology. World Meteorological Organization, Geneva, Switzerland, Operational Hydrology Report No. 40, 60 pp
Kalma JD, Jupp DLB (1990) Estimating evaporation from pasture using infrared thermometry: evaluation of a one-layer resistance model. Agric For Meteorol 51:223–246. doi:10.1016/0168-1923(90)90110-R
Kustas WP (1990) Estimates of evapotranspiration with a one- and two-layer model of heat transfer over partial canopy cover. J Appl Meteorol 29:704–715. doi :10.1175/1520-0450(1990)029<0704:EOEWAO>2.0.CO;2
Kustas WP (2000) Recent advances in the application of remote sensing for monitoring land surface fluxes. In: McVicar TR (ed) Proceedings Land EnvSat Workshop, 10th Australasian remote sensing and photogrammetry conference, Adelaide, August 2000, pp 29–39 http://www.clw.csiro.au/publications/technical2000/tr36-00.pdf
Kustas WP, Norman JM (1996) Use of remote sensing for evapotranspiration monitoring over land surfaces. Hydrol Sci J 41(4):495–516
Kustas WP, Norman JM (1999) Evaluation of soil and vegetation heat flux predictions using a simple two-source model with radiometric temperatures for partial canopy cover. Agric For Meteorol 94:13–29. doi:10.1016/S0168-1923(99)00005-2
Kustas WP, Moran MS, Humes KS, Stannard DI, Pinter PJ, Hipps LE (1994a) Surface energy balance estimates at local and regional scales using optical remote sensing from aircraft platforms and

atmospheric data collected over semiarid rangelands. Water Resour Res 30(5):1241–1259. doi:10.1029/93WR03038

Kustas WP, Perry EM, Doraiswamy PC, Moran MS (1994b) Using satellite remote sensing to extrapolate evapotranspiration estimates in space and time over a semi-arid rangeland basin. Remote Sens Environ 49:275–286. doi:10.1016/0034-4257(94)90022-1

Kustas WP, French AN, Hatfield JL, Jackson TJ, Moran MS, Rango A (2003a) Remote sensing research in hydrometeorology. Photogramm Eng Remote Sensing 69(6):613–646

Kustas WP, Norman JM, Schmugge TJ, Anderson MC (2003b) Mapping surface energy fluxes with radiometric temperature. In: Quattrochi DA, Luvall JC (eds) Thermal remote sensing in land surface processes. Taylor and Francis, London

Kustas WP, Norman J, Anderson MC, French AN (2003c) Estimating subpixel surface temperatures and energy fluxes from the vegetation index–radiometric temperature relationship. Remote Sens Environ 85:429–440. doi:10.1016/S0034-4257(03)00036-1

Kustas WP, Li F, Jackson TJ, Prueger JH, MacPherson JI, Wolde M (2004) Effects of remote sensing pixel resolution on modeled energy flux variability of croplands in Iowa. Remote Sens Environ 92:535–547. doi:10.1016/j.rse.2004.02.020

Kustas WP, Hatfield JL, Prueger JH (2005) The Soil Moisture–Atmosphere Coupling Experiment (SMACEX): background, hydrometeorological conditions, and preliminary findings. J Hydrometeorol 6:825–839. doi:10.1175/JHM460.1

Lambin EF, Ehrlich D (1996) The surface temperature–vegetative index space for land cover and land cover change analysis. Int J Remote Sens 17(3):463–487. doi:10.1080/01431169608949021

Lhomme JP, Monteny B, Amadou M (1994) Estimating sensible heat flux from radiometric temperature over sparse millet. Agric For Meteorol 44:197–216

Li F, Kustas WP, Prueger JH, Neale CMU, Jackson TJ (2005) Utility of remote sensing based two-source energy balance model under low and high vegetation cover conditions. J Hydrometeorol 6(6):878–891. doi:10.1175/JHM464.1

Li F, Kustas WP, Anderson MC, Jackson TJ, Bindlish R, Prueger JH (2006) Comparing the utility of microwave and thermal remote-sensing constraints in two-source energy balance modeling over an agricultural landscape. Remote Sens Environ 101:315–328. doi:10.1016/j.rse.2006.01.001

Li F, Kustas WP, Anderson MC, Prueger JH, Scott RL (2008) Effect of remote sensing spatial resolution on interpreting tower-based flux observations. Remote Sens Environ 112:337–349. doi:10.1016/j.rse.2006.11.032

Liu Y, Yamaguchi Y, Ke C (2007) Reducing the discrepancy between ASTER and MODIS land surface temperature products. Sensors 7:3043–3057

Loukas A, Vasiliades L, Domenikiotis C, Dalezios NR (2005) Basin-wide actual evapotranspiration estimation using NOAA/AVHRR satellite data. Phys Chem Earth 30:69–79

Lu H, Raupach MR, McVicar TR, Barrett DJ (2003) Decomposition of vegetation cover into woody and herbaceous components using AVHRR NDVI time series. Remote Sens Environ 86:1–18. doi:10.1016/S0034-4257(03)00054-3

Massman WJ (1997) An analytical one-dimensional model of momentum transfer by vegetation of arbitrary structure. Boundary-Layer Meteorol 83:407–421. doi:10.1023/A:1000234813011

McCabe MF, Wood EF (2006) Scale influences on the remote estimation of evapotranspiration using multiple satellite sensors. Remote Sens Environ 105(4):271–285. doi:10.1016/j.rse.2006.07.006

McCabe MF, Franks SW, Kalma JD (2005a) Calibration of a land surface model using multiple data sets. J Hydrol (Amst) 302(1–4):209–222. doi:10.1016/j.jhydrol.2004.07.002

McCabe MF, Kalma JD, Franks SW (2005b) Spatial and temporal patterns of land surface fluxes from remotely sensed surface temperatures within an uncertainty framework. Hydrol Earth Syst Sci 9:467–480

McCabe MF, Balick L, Theiler JP, Gillespie AR, Mushkin A (2008a) Linear mixing in thermal IR temperature retrieval. Int J Remote Sens (in press)

McCabe MF, Wood EF, Wójcik R, Pan M, Sheffield J, Gao H (2008b) Hydrological consistency using multi-sensor remote sensing data for water and energy cycle studies. Remote Sens Environ 112(2):430–444. doi:10.1016/j.rse.2007.03.027

McVicar TR, Bierwirth PN (2001) Rapidly assessing the 1997 drought in papua new guinea using composite AVHRR imagery. Int J Remote Sens 22:2109–2128. doi:10.1080/01431601300190631

McVicar TR, Jupp DLB (1998) The current and potential operational uses of remote sensing to aid decisions on drought exceptional circumstances in Australia: a review. Agric Syst 57:399–468. doi:10.1016/S0308-521X(98)00026-2

McVicar TR, Jupp DLB (1999) Estimating one-time-of-day meteorological data from standard daily data as inputs to thermal remote sensing based energy balance models. Agric For Meteorol 96:219–238. doi:10.1016/S0168-1923(99)00052-0

McVicar TR, Jupp DLB (2002) Using covariates to spatially interpolate moisture availability in the Murray Darling Basin: a novel use of remotely sensed data. Remote Sens Environ 79:199–212. doi:10.1016/S0034-4257(01)00273-5

McVicar TR, Van Niel TG, LingTao Li, Hutchinson MF, XingMin Mu, ZhiHong Liu (2007a) Spatially distributing monthly reference evapotranspiration and pan evaporation considering topographic influences. J Hydrol (Amst) 338:196–220. doi:10.1016/j.jhydrol.2007.02.018

McVicar TR, Van Niel TG, Li LT, King EA, Donohue RJ (2007b) Deriving moisture availability from time series remote sensing for ecohydrological applications: development of a prototype near real-time operational system. CSIRO Land and Water Science Report 37/07, Canberra, Australia, 144 pp. http://www.clw.csiro.au/publications/science/2007/sr37-07.pdf

McVicar TR, Li LT, Van Niel TG, Zhang L, Li R, Yang QK (2007c) Developing a decision support tool for China's re-vegetation program: simulating regional impacts of afforestation on average annual streamflow in the Loess Plateau. For Ecol Manage 251:65–81. doi:10.1016/j.foreco.2007.06.025

Mecikalski JR, Diak GR, Anderson MC, Norman JM (1999) Estimating fluxes on continental scales using remotely sensed data in an atmospheric-land exchange model. J Appl Meteorol 38:1352–1369. doi :10.1175/1520-0450(1999)038<1352:EFOCSU>2.0.CO;2

Monteith JL (1965) Evaporation and the environment. In: Fogg GE (ed) The state and movement of water in living organisms, 19th symposium of the society for experimental biology. University Press, Cambridge, pp 205–234

Moran MS, Jackson RD (1991) Assessing the spatial distribution of evapotranspiration using remotely sensed inputs. J Environ Qual 20:725–737

Moran MS, Jackson RD, Raymond LH, Gay LW, Slater PN (1989) Mapping surface energy balance components by combining Landsat Thematic mapper and ground-based meteorological data. Remote Sens Environ 30:77–87. doi:10.1016/0034-4257(89)90049-7

Moran MS, Clarke TR, Inoue Y, Vidal A (1994) Estimating crop water deficit using the relation between surface–air temperature and spectral vegetation index. Remote Sens Environ 49:246–263. doi:10.1016/0034-4257(94)90020-5

Moran MS, Humes KS, Pinter PJ (1997) The scaling characteristics of remotely-sensed variables for sparsely-vegetated heterogeneous surfaces. J Hydrol (Amst) 190:337–362. doi:10.1016/S0022-1694(96)03133-2

Nagler PL, Cleverly J, Glenn E, Lampkin D, Huete A, Wan Z (2005a) Predicting riparian evapotranspiration from MODIS vegetation indices and meteorological data. Remote Sens Environ 94(1):17–130. doi:10.1016/j.rse.2004.08.009

Nagler PL, Scott RL, Westenburg C, Cleverly JR, Glenn EP, Huete AR (2005b) Evapotranspiration on western US rivers estimated using the enhanced vegetation indices from MODIS and data from eddy covariance and Bowen ratio flux towers. Remote Sens Environ 97(3):337–351. doi:10.1016/j.rse.2005.05.011

Nagler PL, Glenn E, Kim H, Emmerich W, Scott R, Huxman T (2007) Seasonal and interannual variation of ET for a semiarid watershed estimated by moisture flux towers and MODIS vegetation indices. J Arid Environ 70(3):443–462. doi:10.1016/j.jaridenv.2006.12.026

Nemani R, Running SW (1989) Estimation of regional surface resistance to evapotranspiration from NDVI and thermal-IR AVHRR data. J Appl Meteorol 28:276–284. doi :10.1175/1520-0450(1989)028<0276:EORSRT>2.0.CO;2

Nishida K, Nemani RR, Running SW, Glassy JM (2003a) An operational remote sensing algorithm of land surface evaporation. J Geophys Res 108, No. D9, 4270. (doi:101029/2002JD002062)

Nishida K, Nemani RR, Glassy JM, Running SW (2003b) Development of an evapotranspiration index from Aqua/MODIS for monitoring surface moisture status. IEEE Trans Geosci Rem Sens 41:493–501. doi:10.1109/TGRS.2003.811744

Noilhan JM, Mahfouf JF (1996) The ISBA land surface parameterization scheme. Global Planet Change 13:145–159. doi:10.1016/0921-8181(95)00043-7

Norman JM, Becker F (1995) Terminology in thermal infrared remote sensing of natural surfaces. Agric For Meteorol 77:153–166. doi:10.1016/0168-1923(95)02259-Z

Norman JM, Kustas WP, Humes KS (1995) A two-source approach for estimating soil and vegetation energy fluxes from observations of directional radiometric surface temperature. Agric For Meteorol 77:263–293. doi:10.1016/0168-1923(95)02265-Y

Norman JM, Kustas WP, Prueger JH, Diak GR (2000) Surface flux estimation using radiometric temperature: a dual-temperature-difference method to minimize measurement errors. Water Resour Res 36:2263–2274. doi:10.1029/2000WR900033

Norman JM, Anderson MC, Kustas WP, French AN, Mecikalski JR, Torn RD (2003) Remote sensing of surface energy fluxes at 10^1-m resolutions. Water Resour Res 39(8):1221. doi:10.1029/2002WR001775

Nunez M, Kalma JD (1995) Satellite mapping of the surface radiation budget. Adv Bioclimatology 4:63–124

Olioso A, Inoue Y, Demarty J, Wigneron JP, Braud I, Ortega-Farias S (2002a) Assimilation of remote sensing data into crop simulation models and SVAT models. In: Sobrino JA (ed) Proceedings of 1st international symposium on recent advances in quantitative remote sensing, Valencia, 16–18 September 2002, pp 329–338

Olioso A, Hasager C, Jacob F, Wassenaar T, Chehbouni A, Maloie O (2002b) Mapping surface flux from thermal infrared and reflectance data using various models over the Arpilles test site. In: Sobrino JA (ed) Proceedings of 1st international symposium on recent advances in quantitative remote sensing, Valencia, 16–18 September 2002, pp 450–457

Ottlé C, Vidal-Madjar D (1994) Assimilation of soil moisture inferred from remote sensing in a hydrological model over the HAPEX-MOBILHY region. J Hydrol (Amst) 158:241–264. doi:10.1016/0022-1694(94)90056-6

Overgaard J, Rosbjerg D, Butts MB (2006) Land-surface modelling in hydrological perspective—a review. Biogeosciences 3:229–241

Pan M, Wood EF (2006) Data assimilation for estimating land water budget using a constrained ensemble Kalman filter. J Hydrometeorol 7(3):534–547. doi:10.1175/JHM495.1

Pan M, Wood EF, Wójcik R, McCabe MF (2008) Estimation of the regional terrestrial water cycle using multi-sensor remote sensing observations and data assimilation. Remote Sens Environ 112(4):1282–1294. doi:10.1016/j.rse.2007.02.039

Penman HL (1948) Natural evaporation from open water, bare soil and grass. Proc R Soc Lond A Math Phys Sci 193:120–146. doi:10.1098/rspa.1948.0037

Pereira AR (2004) The Priestley–Taylor parameter and the decoupling factor for estimating reference evapotranspiration. Agric For Meteorol 125:305–313. doi:10.1016/j.agrformet.2004.04.002

Pinter PJ Jr (1986) Effect of dew on canopy reflectance and temperature. Remote Sens Environ 19:187–205. doi:10.1016/0034-4257(86)90071-4

Prata AJ (1993) Land surface temperatures derived from the Advanced Very High Resolution Radiometer and the Along-Track Scanning Radiometer 1. Theory. J Geophys Res 98:16,689–16,702. doi:10.1029/93JD01206

Prata AJ (1994) Land surface temperature derived from the Advanced Very High Resolution Radiometer and the Along-Track Scanning Radiometer 2 Experimental results and validation of AVHRR algorithms. J Geophys Res 99:13,025–13,058. doi:10.1029/94JD00409

Priestley CHB, Taylor RJ (1972) On the assessment of surface heat flux and evaporation using large scale parameters. Mon Weather Rev 100:81–92. doi :10.1175/1520-0493(1972)100<0081:OTAOSH>2.3.CO;2

Pypker TG, Unsworth MH, Mix AC, Rugh W, Ocheltree T, Alstad K (2007) Using nocturnal cold air drainage flow to monitor ecosystem processes in complex terrain. Ecol Appl 17(3):702–714. doi:10.1890/05-1906

Quattrochi DA, Luvall FJC (1999) Thermal infrared remote sensing for analysis of landscape ecological processes: methods and applications. Landscape Ecol 14:577–598. doi:10.1023/A:1008168910634

Raupach MR, Finnigan JJ (1988) 'Single-layer models of evaporation from plant canopies are incorrect but useful, whereas multilayer models are correct but useless': discuss. Aust J Plant Physiol 15:705–716

Renzullo LJ, Barrett DJ, Marks AS, Hill MJ, Guerschman JP, Mu Q (2008) Multi-sensor model-data fusion for estimation of hydrologic and energy flux parameters. Remote Sens Environ 112:1306–1319. doi:10.1016/j.rse.2007.06.022

Rodell M, Famiglietti JS, Chen J, Seneviratne SI, Viterbo P, Holl S (2004) Basin scale estimates of evapotranspiration using GRACE and other observations. Geophys Res Lett 31:L20504. doi:10.1029/2004GL020873

Roderick ML, Farquhar GD, Berry SL, Noble IR (2001) On the direct effect of clouds and atmospheric particles on the productivity and structure of vegetation. Oecologia 129:21–30. doi:10.1007/s004420100760

Roderick ML, Rotstayn LD, Farquhar GD, Hobbins MT (2007) On the attribution of changing pan evaporation. Geophys Res Lett 34:L17403. doi:10.1029/2007GL031166

Roerink GJ, Su Z, Menenti M (2000) S-SEBI: a simple remote sensing algorithm to estimate the surface energy balance. Phys Chem Earth, Part B Hydrol Oceans Atmos 25(2):147–157. doi:10.1016/S1464-1909(99)00128-8

Sanchez JM, Kustas WP, Caselles V, Anderson M (2007) Modelling surface energy fluxes over maize using radiometric soil and canopy temperature observations. Remote Sens Environ. doi:10.1016/j.rse.2007.07.018

Sanchez JM, Scavone G, Caselles V, Valor E, Copertino VA, Telesca V (2008) Monitoring daily evapotranspiration at a regional scale from Landsat-TM and ETM + data: application to the Basilicata region. J Hydrol 351:58–70. doi:10.1016/j.jhydrol.2007.11.041

Schmidt M, King EA, McVicar TR (2006) A user-customized Web-based delivery system of hypertemporal remote sensing datasets for Australasia. Photogramm Eng Remote Sensing 72:1073–1080

Schmugge TJ, Becker F (1991) Remote sensing observations for the monitoring of land surface fluxes and water budgets. In: Schmugge TJ, Andre JC (eds) Land surface evaporation: measurement and parameterization. Springer Verlag, Berlin, pp 337–347

Schüttemeyer D, Schillings C, Moene AF, de Bruin HAR (2007) Satellite-based actual evapotranspiration over drying semiarid terrain in West Africa. J Appl Meteorol Climatol 46:97–111. doi:10.1175/JAM2444.1

Seguin B, Itier B (1983) Using midday surface temperatures to estimate daily evaporation from satellite thermal IR data. Int J Remote Sens 4(2):371–383. doi:10.1080/01431168308948554

Seguin B, Baelz S, Monget JM, Petit V (1982a) Utilisation de la thermographie IR pour l'estimation de l'évaporation régionale I Mise au point méthodologique sur le site de la Crau. Agronomie 2(1):7–16. doi:10.1051/agro:19820102

Seguin B, Baelz S, Monget JM, Petit V (1982b) Utilisation de la thermographie IR pour l'estimation de l'évaporation régionale II Résultats obtenues à partir des données de satellite. Agronomie 2(2):113–118. doi:10.1051/agro:19820202

Seguin B, Becker F, Phulpin T, Gu XF, Guyot G, Kerr Y (1999) IRSUTE: a minisatellite project for land surface heat flux estimation from field to regional scale. Remote Sens Environ 68:357–369. doi:10.1016/S0034-4257(98)00122-9

Sellers PJ, Rasool SI, Bolle HJ (1990) A review of satellite data algorithms for studies of the land surface. Bull Am Meteorol Soc 71:1429–1447. doi :10.1175/1520-0477(1990)071<1429:AROSDA>2.0.CO;2

Shuttleworth WJ (1991) Insight from large scale observational studies of land/atmosphere interactions. In: Wood EF (ed) Land surface–atmosphere interactions for climate modelling. Surv Geophys 12(1–3):3–31

Shuttleworth WJ, Wallace JS (1985) Evaporation from sparse crops-an energy combination theory. Q J R Meteorol Soc 111:839–855. doi:10.1256/smsqj.46909

Sobrino JA, Gomez M, Jimenez-Munoz JC, Olioso A (2007) Application of a simple algorithm to estimate daily evapotranspiration from NOAA-AVHRR images for the Iberian Peninsula. Remote Sens Environ 110:139–148. doi:10.1016/j.rse.2007.02.017

Stewart JB, Kustas WP, Humes KS, Nichols WD, Moran MS, De Bruin HAR (1994) Sensible heat flux–radiometric surface temperature relationships for eight semi-arid areas. J Appl Meteorol 33:1110–1117. doi :10.1175/1520-0450(1994)033<1110:SHFRST>2.0.CO;2

Su Z (2002) The Surface Energy Balance System (SEBS) for estimation of turbulent heat fluxes. Hydrol Earth Syst Sci 6(1):85–99 (HESS)

Su H, McCabe MF, Wood EF, Su Z, Prueger JH (2005) Modeling evapotranspiration during SMACEX: comparing two approaches for local- and regional-scale prediction. J Hydrometeorol 6(6):910–922. doi:10.1175/JHM466.1

Su H, Wood EF, McCabe MF, Su Z (2007) Evaluation of remotely sensed evapotranspiration over the CEOP EOP-1 reference sites. J Meteorol Soc Jpn 85A:439–459. doi:10.2151/jmsj.85A.439

Suggs RJ, Jedlovic GJ, Lapenta WM (1999) Satellite derived land surface temperatures for model assimilation. In: Proceedings 3rd symposium on integrated observing systems, American Meteorological Society, Dallas, pp 205–208

Sun NZ (1994) Inverse problems in groundwater modelling. Kluwer Academic Publisher, Dordrecht, 337 pp

Taconet O, Bernard R, Vidal-Madjar D (1986) Evapotranspiration over an agricultural region using a surface flux/temperature model based on NOAA-AVHRR data. J Clim Appl Meteorol 25:284–307. doi :10.1175/1520-0450(1986)025<0284:EOAARU>2.0.CO;2

Timmermans WJ, Kustas WP, Anderson MC, French AN (2007) An intercomparison of the Surface Energy Balance Algorithm for Land (SEBAL) and Two-Source Energy Balance (TSEB) modelling schemes. Remote Sens Environ 108(4):369–384. doi:10.1016/j.rse.2006.11.028

Tittebrand A, Schwieben A, Berger F (2005) The influence of land surface parameters on energy flux densities derived from remote sensing data. Meteorologische Zeitschrift 14:227–236

Troufleau D, Lhomme JP, Monteny B, Vidal A (1997) Sensible heat flux and radiometric temperature over sparse Sahelian vegetation. 1: an experimental analysis of the kB^{-1} parameter. J Hydrol (Amst) 188/189(1–4):815–838. doi:10.1016/S0022-1694(96)03172-1

Twine TE, Kustas W, Norman J, Cook D, Houser P, Meyers TP (2000) Correcting eddy-covariance flux underestimates over a grassland. Agric For Meteorol 103(3):279–300. doi:10.1016/S0168-1923(00)00123-4

Van den Hurk BJJM, Bastiaanssen WGM, Pelgrum H, Van Meijgaard E (1997) A new methodology for assimilation of initial soil moisture fields in weather prediction models using METEOSAT and NOAA data. J Appl Meteorol 36:1271–1283. doi :10.1175/1520-0450(1997)036<1271:ANMFAO>2.0.CO;2

Van Niel TG, McVicar TR (2003) A simple method to improve field-level rice identification: toward operational monitoring with satellite remote sensing. Aust J Exp Agric 43:379–387. doi:10.1071/EA02182

Van Niel TG, McVicar TR (2004a) Current and potential uses of optical remote sensing in rice-based irrigation systems: a review. Aust J Agric Res 55:155–185. doi:10.1071/AR03149

Van Niel TG, McVicar TR (2004b) Determining temporal windows of crop discrimination with remote sensing: a case study in south-eastern Australia. Comput Electron Agric 45:91–108. doi:10.1016/j.compag.2004.06.003

Van Niel TG, McVicar TR, Fang HL, Liang S (2003) Calculating environmental moisture for per-field discrimination of rice crops. Int J Remote Sens 24:885–890. doi:10.1080/0143116021000009921

Venturini V, Bisht G, Islam S, Jiang L (2004) Comparison of evaporative fractions estimated from AVHRR and MODIS sensors over South Florida. Remote Sens Environ 93:77–86. doi:10.1016/j.rse.2004.06.020

Venturini V, Islam S, Rodriguez L (2008) Estimation of evaporative fraction and evapotranspiration from MODIS products using a complementary based model. Remote Sens Environ 112:132–141. doi:10.1016/j.rse.2007.04.014

Verstraeten WW, Veroustraete F, Feyen J (2005) Estimating evapotranspiration of European forests from NOAA-imagery at satellite overpass time: towards an operational processing chain for integrated optical and thermal sensor data products. Remote Sens Environ 96:256–276. doi:10.1016/j.rse.2005.03.004

Verstraeten WW, Veroustraete F, Feyen J (2008) Assessment of evapotranspiration and soil moisture content across different scales of observation. Sensors 8:70–117

Vose RS, Easterling DR, Gleason B (2005) Maximum and minimum temperature trends for the globe: An update through 2004. Geophys Res Lett 32:L23822. doi:10.1029/2005GL024379

Vrugt JA, Gupta HV, Bastidas LA, Bouten W, Sorooshian S (2003) Effective and efficient algorithm for multiobjective optimization of hydrologic models. Water Resour Res 39(8):1214. doi:10.1029/2002WR001746

Walker JP, Houser PR (2001) A methodology for initializing soil moisture in a global climate model: Assimilation of near-surface soil moisture observations. J Geophys Res 106(D11):11,761–11,774. doi:10.1029/2001JD900149

Wan Z, Zhang Y, Zhang Q, Li Z (2004) Quality assessment and validation of the MODIS global land surface temperature. Int J Remote Sens 25:261–274. doi:10.1080/0143116031000116417

Wang K, Li Z, Cribb M (2006) Estimation of evaporative fraction from a combination of day and night land surface temperature and NDVI: a new method to determine the Priestley–Taylor parameter. Remote Sens Environ 102:293–305. doi:10.1016/j.rse.2006.02.007

Wang K, Wang P, Li Z, Cribb M, Sparrow M (2007) A simple method to estimate actual evapotranspiration from a combination of net radiation, vegetation index and temperature. J Geophys Res 112:D15107. doi:10.1029/2006JD008351

Wetzel PJ, Atlas D, Woodward R (1984) Determining soil moisture from geosynchronous satellite infrared data: A feasibility study. J Clim Appl Meteorol 23:375–391. doi :10.1175/1520-0450(1984)023<0375:DSMFGS>2.0.CO;2

Wigneron JP, Calvet JC, Kerr Y (1996) Monitoring water interception by crop fields from passive microwave observations. Agric For Meteorol 80:177–194. doi:10.1016/0168-1923(95)02296-1

Wild M, Gilgen H, Roesch A, Ohmura A, Long CN, Dutton EG (2005) From dimming to brightening: decadal changes in solar radiation at earth's surface. Science 308(5723):847–850. doi:10.1126/science.1103215

Wilson K, Falge E, Aubinet M, Baldocchi D, Goldstein A, Berbigier P (2002) Energy balance closure at FLUXNET sites. Agric For Meteorol 113:223–243. doi:10.1016/S0168-1923(02)00109-0

Zhang YC, Rossow WB, Lacis AA (1995) Calculation of surface and top-of-atmosphere radiative fluxes from physical quantities based on ISCCP data sets: 1 Methods and sensitivity to input data uncertainties. J Geophys Res Atmosphere 100(1):1149–1165. doi:10.1029/94JD02747